



A New Local Debonding Model With Application to the Transverse Tensile and Creep Behavior of Continuously Reinforced Titanium Composites

Brett A. Bednarczyk
Ohio Aerospace Institute, Brook Park, Ohio

Steven M. Arnold
Glenn Research Center, Cleveland, Ohio

National Aeronautics and
Space Administration

Glenn Research Center

Acknowledgments

The authors thank Dr. Cheryl L. Bowman of NASA Glenn Research Center for providing the experimental data presented in this report and for several helpful discussions. This work was supported by NASA Contract NCC3-650.

Trade names or manufacturers' names are used in this report for identification only. This usage does not constitute an official endorsement, either expressed or implied, by the National Aeronautics and Space Administration.

Available from

NASA Center for Aerospace Information
7121 Standard Drive
Hanover, MD 21076
Price Code: A03

National Technical Information Service
5285 Port Royal Road
Springfield, VA 22100
Price Code: A03

Available electronically at <http://gltrs.grc.nasa.gov/GLTRS>

A NEW LOCAL DEBONDING MODEL WITH APPLICATION TO THE TRANSVERSE TENSILE AND CREEP BEHAVIOR OF CONTINUOUSLY REINFORCED TITANIUM COMPOSITES

Brett A. Bednarczyk
Ohio Aerospace Institute
Brookpark, Ohio 44142

Steven M. Arnold
National Aeronautics and Space Administration
Glenn Research Center
Cleveland, Ohio 44135

Abstract

A new, widely applicable model for local interfacial debonding in composite materials is presented. Unlike its direct predecessors, the new model allows debonding to progress via unloading of interfacial stresses even as global loading of the composite continues. Previous debonding models employed for analysis of titanium matrix composites are surpassed by the accuracy, simplicity, and efficiency demonstrated by the new model. The new model was designed to operate seamlessly within NASA Glenn's Micromechanics Analysis Code with Generalized Method of Cells (**MAC/GMC**), which was employed to simulate the time- and rate-dependent (viscoplastic) transverse tensile and creep behavior of SiC/Ti composites. **MAC/GMC**'s ability to simulate the transverse behavior of titanium matrix composites has been significantly improved by the new debonding model. Further, results indicate the need for a more accurate constitutive representation of the titanium matrix behavior in order to enable predictions of the composite transverse response, without resorting to recalibration of the debonding model parameters.

1. Introduction

Accurate design and life prediction tools for advanced multi-phased materials are needed to facilitate the implementation of these developing materials. Although closure has not been reached regarding the best models for use in the design and life prediction tools, it has become clear that if a model is ever to serve a purpose beyond that of basic research, it must fulfill several primary requirements. These include a high level of accuracy on the macro and micro scales, computational efficiency, and compatibility with the finite element method. Fulfillment of these requirements allows a model to serve the materials scientists who design the composite materials by enabling quick and easy variation of composite parameters for material development optimization purposes. Likewise, those who design structures with these materials are well served if the model is consistent with the finite element method. Though it is not perfect, the generalized method of cells (**GMC**), developed by Aboudi (1991; 1995), is an excellent choice for implementation into modeling tools for advanced composites, given the requirements described above.

GMC is an analytical micromechanics model for multi-phased materials with arbitrary periodic microstructures. It provides closed-form constitutive equations for such materials and allows easy incorporation of physically based viscoplastic deformation models, as well as arbitrary failure and damage models for each phase. Further, recent independent advances have simplified the utilization of **GMC** as an elemental constitutive model from within commercial nonlinear finite element analyses (Wilt et al., 1997; Arnold et al., 1999), and significantly increased the model's computational efficiency (Pindera and Bednarczyk, 1999).

GMC has been implemented in NASA's comprehensive micromechanics analysis code, **MAC/GMC** (Arnold et al., 1999). The code has many features that render it useful for design, deformation modeling, and life prediction for a wide range of materials. These features include: 1) the

ability to simulate general thermomechanical loading on composites whose geometries are represented by a library of continuous and discontinuous repeating unit cells, 2) a library of nonisothermal elastic/viscoplastic constitutive models, 3) fatigue damage analysis, 4) yield surface analysis, 5) laminate analysis, and 6) interface modeling. The present investigation extends the capabilities of **MAC/GMC** further by incorporating a new physically based micro-level debonding model which allows local unloading to occur in the composite. The code, with this new debonding model, was employed to examine the longitudinal tensile deformation and failure behavior of SiC/Ti composites by Bednarczyk and Arnold (2000). Herein the new debonding model, as implemented in **MAC/GMC**, is applied to examine the transverse tensile deformation and creep behavior of SiC/Ti. The new debonding model is compared with several previous models that have been used to simulate interfacial debonding in titanium matrix composites (TMCs). Via comparison with experiment, it is shown that the new model, working in the context of the recently developed computationally efficient version of **GMC**, allows more accurate modeling of the composite behavior compared to previous methods.

2. The Transverse Response of SiC/Ti Composites

In recent years, the pursuit of advanced aerospace systems has fueled research on TMCs. These materials, in particular continuously reinforced SiC/Ti, have demonstrated potential for high temperature propulsion and airframe application because of their excellent properties at elevated temperature *in the fiber direction*. Unfortunately, the transverse behavior of TMCs has proven to be the composite's Achilles' heel. Weak bonding at the fiber matrix interface renders the composite inferior to monolithic titanium and superalloys in the transverse direction. Amelioration of SiC/Ti transverse properties through lamination of plies with different fiber orientations has proven largely ineffective because the transverse behavior of each ply is so poor. Thus realization of the potential demonstrated by TMCs will likely depend on future development of manufacturing processes that can reduce the effects of the weak bonding in the composite; one example being the hybridization of strong and weakly bonded fibers (Arnold et al., 1996a). In the meantime, modeling efforts, such as the present investigation, can help provide a better understanding of the interface and how the weak bonding affects the overall behavior of TMCs. Further, since the weak bonding in SiC/Ti is so pronounced and so well established, SiC/Ti can serve as a model system for development of interface modeling technology. This technology will then be employed for present and future composite systems that exhibit weak bonding, but are not rendered so ineffective by the weak bonding as TMCs have been thus far.

Figure 1 shows the typical 650 °C tensile response of the SCS-6 fiber, the TIMETAL 21S¹ matrix, and SCS-6/TIMETAL 21S composites in the longitudinal and transverse directions. Evident in the composite transverse response is the characteristic three-stage stress-strain behavior identified by Majumdar and Newaz (1992). Stage I is characterized by the linear elastic behavior of both phases while the fiber-matrix interfaces remain bonded. Stage II begins at the knee in the stress-strain curve, which is caused by interfacial debonding. During stage II the interfaces in the composite are debonding and opening while in the matrix, inelastic deformation begins. In stage III, the interfaces continue to open and the matrix undergoes significant inelastic deformation. While the results shown in Fig. 1 are for the SCS-6/TIMETAL 21S system at 650 °C, the qualitative nature of the transverse response is typical of TMCs in general over a wide range of temperatures (see Nimmer et al., 1991; Lerch and Saltsman, 1993; Brindley and Draper, 1993; Cervay, 1994; Bowman, 1999).

Early work by Karlak et al. (1974) predates the development of SiC/Ti composites, but these authors performed relevant finite element analyses of the transverse tensile behavior of boron/aluminum composites with both perfect bonding and no interfacial adhesion. Although residual stresses from fabrication were not included in the investigation of Karlak et al. (1974), the results clearly showed that weak interfacial bonding in MMCs can result in poor transverse properties compared to the well bonded

¹TIMETAL 21S is a registered trademark of TIMET, Titanium Metals Corporation, Toronto, OH.

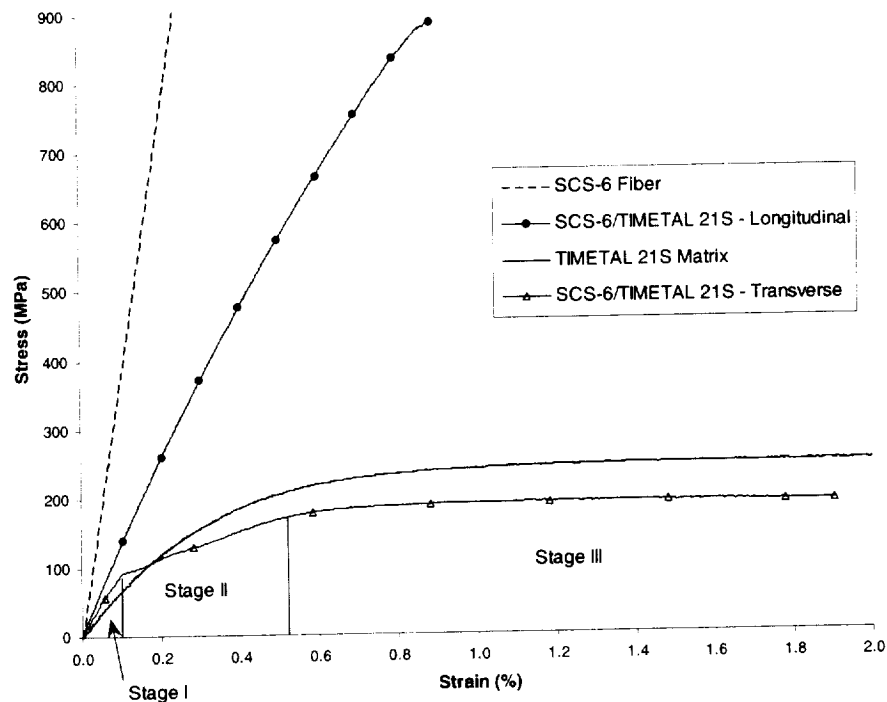


Figure 1: Typical 650 °C tensile response of SCS-6/TIMETAL 21S composites and the constituents. Data courtesy of C.L. Bowman.

case, and even compared to the pure matrix response. Further, Karlak et al. (1974) showed that under transverse tension interfacial debonding should progress to an angle of approximately 75° from the applied stress direction, at which point the stress component normal to the interface becomes compressive (thus disallowing further debonding).

A banner finite element study of SCS-6/Ti-6-4 by Nimmer et al. (1991) shed further light on weakly bonded MMC interfaces. In this investigation, residual stresses from fabrication that led to a state of residual compression at the fiber-matrix interface were included. Upon application of transverse tensile loading, the interfacial stress was required to overcome this residual interfacial clamping before separation (debonding) of the interface could occur. The point at which this simulated debonding occurred gave rise to the characteristic knee in the transverse SiC/Ti response that constitutes the transition between deformation stages I and II (see Fig. 1). It was thus concluded that the knee is due, in a large part, to the presence of the compressive interfacial residual stress that must be overcome for debonding to occur.

Two important characteristics of the work of Nimmer et al. (1991) are its use of a *time-independent* inelasticity model for the Ti-6-4 matrix and its lack of bond strength for the interface. The transverse tensile simulations presented in the paper consistently underpredicted the knee associated with interfacial debonding evident in experimental results (by up to 15%). This suggests that the fiber-matrix interface has some strength, as the presence of this strength in the analysis would have raised the knee to better agree with experiment. Further, Nimmer et al. (1991) indicated that the time-independent inelasticity model probably led to an overprediction of the compressive residual stress magnitude (by approximately 16%) because it did not allow the residual stress arising in the matrix to relax at elevated temperature. Inclusion of matrix relaxation in the simulations would have tended to lower the compressive residual stress magnitude and thus lower the simulated knee further. This lends additional credence to the theory that the SiC/Ti interface exhibits some degree of chemical bonding in addition to the residual mechanical clamping indicated by the Nimmer et al. (1991) investigation. The work of Hu

(1996) and Warrier et al. (1999) also points to the existence of a chemical interfacial bond at the SiC/Ti interface.

A final point elucidated by Nimmer et al. (1991) is the importance of constituent material modeling and characterization, so as to simulate accurately the SiC/Ti transverse response. The authors discussed the significant variation (up to 20%) in coefficient of thermal expansion (CTE) data reported for Ti-6-4 in material property guides and showed that such variations have a significant effect on the predicted residual clamping at the fiber-matrix interface. The authors also discussed the importance of matrix relaxation, which their matrix constitutive model did not admit, leading to additional variations in the residual stress field. Similarly, the residual stress field was shown to be a major determinant of the location of the debonding knee, which is the single most important characteristic of the TMC transverse response. The weight of this evidence (as well as the results presented herein and in Goldberg and Arnold (2000)) point to two conclusions: 1) accurate constituent characterization is critical to the simulation of transverse TMC behavior, and 2) a chemical bond is present in TMCs and must be incorporated in the composite's analysis. For modeling composites in which local fields only influence the global response in an average way (i.e., longitudinal deformation, well-bonded composites), this characterization is far less critical. However, when significant features of the composite's global response are driven by the local fields (such as the interfacial stress), high fidelity constitutive models and constitutive model parameters are required in order to have any chance at simulating the global response accurately.

A good deal of work has been performed on simulating the transverse response of TMCs using analytical models, in particular, Aboudi's (1991) method of cells and its generalization (**GMC**) (Aboudi, 1995). An in-depth discussion of several of the approaches employed in these studies is given in the next section.

3. Interfacial Debonding Models

The interfacial debonding models reviewed and compared in this section have all been incorporated into Aboudi's method of cells or **GMC**. **GMC** itself is discussed in Section 4. The method is ideal for modeling composites with weak bonding because it provides the local stresses and strains necessary to implement a local debonding model at the fiber-matrix interface. Further, **GMC**'s computational efficiency, as well as its ability to admit arbitrary time-dependent constitutive models for the phases, adds to the model's attractiveness for this endeavor. The final part of this section presents the new interfacial debonding model developed and implemented (in **MAC/GMC**) as part of this investigation.

3.1 Flexible Interface (**FI**) Model

Aboudi (1987) incorporated the flexible interface (**FI**) model of Jones and Whittier (1967) into the method of cells. This model permits a discontinuity in the normal or tangential displacement component at an interface, I , that is proportional to the appropriate stress component at the interface. The normal and tangential displacement discontinuities can be expressed as,

$$[u_n]^I = R_n \sigma_n|^I \quad [u_t]^I = R_t \sigma_t|^I, \quad (1)$$

where R_n and R_t are debonding parameters that represent the effective compliance of the interface. The interfacial constitutive behavior represented by the **FI** model is plotted in Fig. 2. The interface is modeled as flexible for all time. By selecting a large value for the interface debonding parameter, R , a completely debonded condition is simulated. The obvious limitations of the **FI** model are: 1) its lack of a finite interfacial bond strength, and 2) the inability to vary the degree to which the interface can debond as deformation progresses.

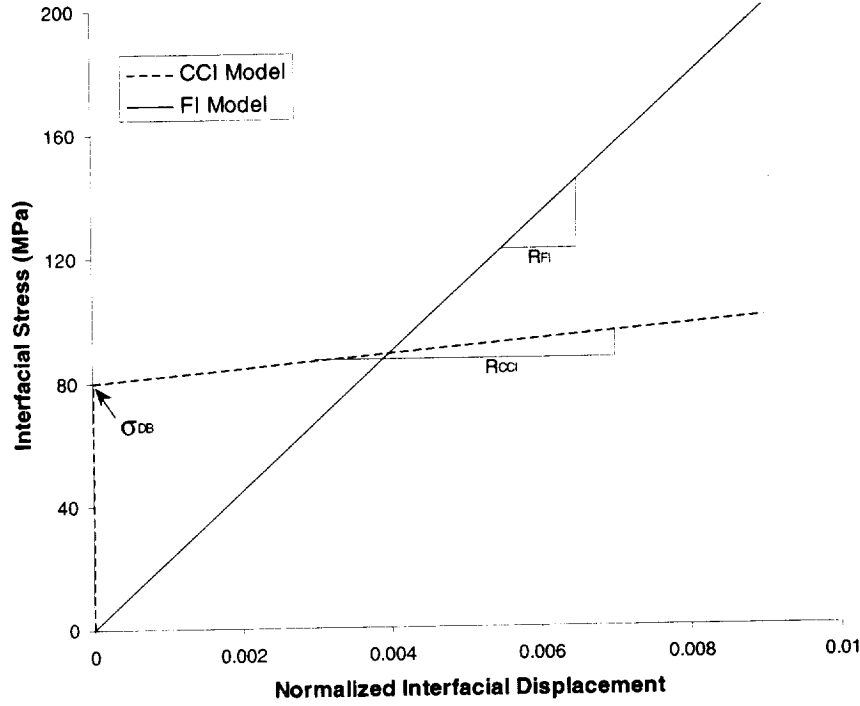


Figure 2: Interfacial constitutive behavior represented by the **FI** and **CCI** models.

3.2 Constant Compliant Interface (**CCI**) Model

The **FI** model concept was employed by Achenbach and Zhu (1989) with an added condition that requires the interfacial compliance to be zero (thus simulating perfect bonding) when the interface is in compression. This modification was further expanded by Wilt and Arnold (1996) who included a finite interfacial strength for the interface, incorporated the model into a rate-based formulation of **GMC**, and employed the following interfacial equations:

$$\begin{aligned} [\dot{u}_n]^I &= R_n \dot{\sigma}_n|^I; & \sigma_n|^I &\geq \sigma_{DB}|^I \\ [\dot{u}_t]^I &= R_t \dot{\sigma}_t|^I; & \sigma_t|^I &\geq \sigma_{DB}|^I \end{aligned} \quad (2)$$

where dots denote time differentiation. Thus, in essence, the interface behaves as perfectly bonded at stresses lower than σ_{DB} and flexible at stresses greater than σ_{DB} . This model will be referred to as the constant compliant interface (**CCI**) model. Inclusion of a finite interfacial strength is a major improvement since, as discussed earlier, previous work on SiC/Ti composites points to the existence of a weak chemical bond at the fiber-matrix interface (Nimmer et al., 1991; Hu, 1996; Warrier et al., 1999). Thus the interfacial stress must not only exceed any mechanical clamping due to compressive residual stress, but also rise into the tensile regime to overcome the chemical bond. However, like the **FI** model, the **CCI** model is limited by the fact that once interfacial debonding occurs, the degree of debonding does not increase (i.e., the parameter R is constant).

The interfacial constitutive behavior for the **CCI** model is shown in Fig. 2. As with the **FI** model, a large value of the debonding parameter can be chosen to simulate a completely debonded interface after failure. The **CCI** model, as implemented in **GMC**, was employed by Goldberg and Arnold (2000) to model the transverse tensile response of SCS-6/TIMETAL 21S. Through comparison with experiment, it

was shown that the **CCI** model allowed improved prediction of the transverse tensile response of SiC/Ti, especially with respect to capturing the knee associated with interfacial debonding. The study also indicated that in the SCS-6/TIMETAL 21S system, a finite chemical bond does exist between the fiber and matrix.

3.3 Needleman Interface (NI) Model

The interface constitutive equations developed by Needleman (1987) were incorporated into the method of cells by McGee and Herakovich (1992). Note that (unfortunately) the study by McGee and Herakovich (1992) was not published in a widely available source. The effective interfacial constitutive behavior represented by the Needleman interface (**NI**) model is shown in Fig. 3. Clearly, this interfacial representation is distinct from the **FI** and **CCI** representations shown in Fig. 2. Unlike these previously discussed interface models, the **NI** model allows the degree of debonding to progress via unloading of the interfacial stress. That is, the interfacial stress first rises and then falls as the global loading and the interfacial displacement continue to increase. This is a major improvement over the previous approaches, as physics demands that a failed interface must locally unload the stress it was supporting as the interface opens. The **NI** model does not, however, include a finite interfacial bond strength. As Fig. 3 shows, the interfacial response is flexible at all points in the tensile regime. This lack of finite bond strength seems to be somewhat inaccurate from a physical standpoint, yet results indicated that the **NI** model, as implemented in the method of cells, allows improved simulation of the transverse tensile response of SCS-6/Ti-6-4 composites (McGee and Herakovich, 1992). However, some difficulties arise in employing the **NI** model as unrealistic “humps” in the simulated composite transverse tensile response tend to occur (see also Section 6.1). This problem was also encountered by Eggleston (1993), who applied the **NI** model to the transverse tensile response of SiC/Ti-6-4 via incorporation into a finite element model.

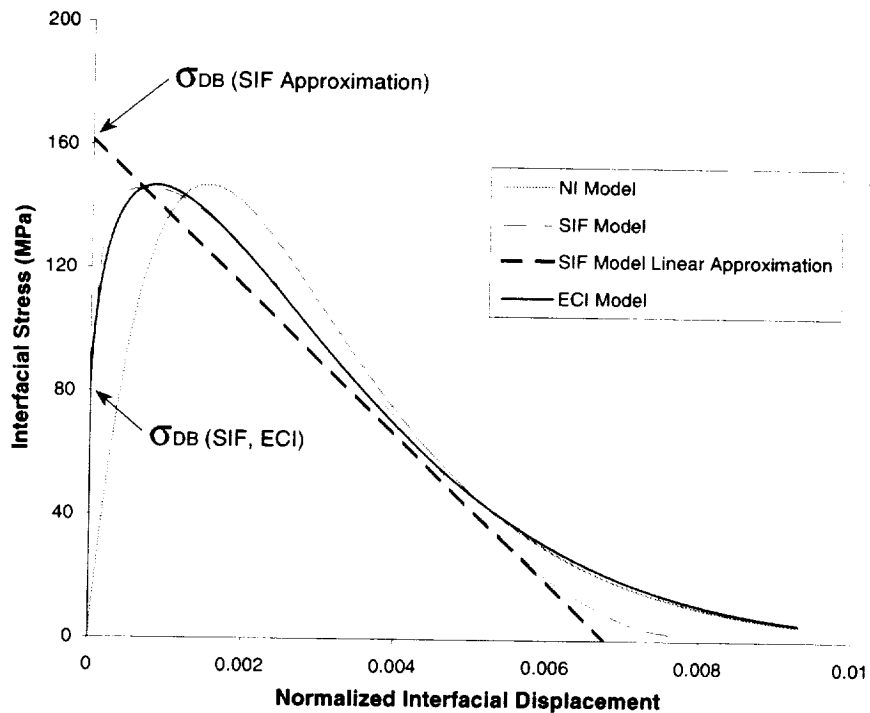


Figure 3: Interfacial constitutive behavior represented by the **NI**, **SIF**, and **ECI** models.

It should be noted that, due to the complexity associated with the **NI** model, incorporation of the model into the method of cells required the introduction of additional *nonlinear* equations for each interface. Thus, the physically motivated shape of the **NI** model constitutive behavior (see Fig. 3) comes at a significant computational cost. In addition, due to the nonlinearity introduced by the **NI** model into the method of cells, closed-form constitutive equations for the weakly bonded composite are not available. Thus, unlike the **FI** and **CCI** model method of cells implementations, effective composite properties are not available when using the **NI** model.

3.4 Statistical Interfacial Failure (**SIF**) Model

Robertson and Mall (1994) developed a statistical interfacial failure (**SIF**) model and incorporated a linear approximation of the interface representation into a modified version of the method of cells. The **SIF** model assumes a Gaussian distribution of interfacial stresses and specifies a single deterministic interfacial failure strength. The portion of the interfacial stress distribution lying above this failure strength represents the failed interfaces at a particular load level. The average interfacial constitutive behavior represented by the **SIF** model is shown in Fig. 3. The similarities between this representation and the **NI** model are obvious. Since below approximately 80 MPa the **SIF** model interface exhibits almost no displacement, this stress value may be thought of as an effective debond stress for the average interface. This characteristic is similar to the **CCI** model, which incorporates an explicit interfacial strength (see Fig. 2). Further, like the **NI** model, the **SIF** model allows the degree of debonding to progress via unloading of the interfacial stress.

Also shown in Fig. 3 is the linear approximation used by Robertson and Mall (1994) to incorporate the **SIF** model into the modified method of cells. Recall that the **NI** model exacted a computational cost due to the complex nature of the interfacial equations. Robertson and Mall (1994) evade a similar cost associated with the **SIF** model by employing this linear approximation of their physically and statistically motivated interfacial response. Clearly the approximation does a reasonable job of capturing the important unloading behavior of the interfacial stress. However, the approximation does not capture the early **SIF** model interfacial behavior. Nevertheless, results presented by Robertson and Mall (1994) indicate that the approximation of the **SIF** model, in conjunction with the modified method of cells, allows improved simulation of the transverse tensile response of SCS-6/Ti-15-3 composites compared to simulations performed with complete and immediate interfacial debonding.

3.5 Evolving Compliant Interface (**ECI**) Model

For the present investigation, a new interfacial debonding model was developed that attempts to combine desirable characteristics of the previous approaches discussed. The new evolving compliant interface (**ECI**) model was incorporated into **GMC** for modeling the transverse tensile response of composite materials. The **ECI** model is similar to the **FI** and **CCI** models in that it is based on the Jones and Whittier (1967) concept of incorporating a flexible interface via interfacial displacement discontinuities. Further, like the **NI** and **SIF** models, the **ECI** model allows progression of the debonding via unloading of the interfacial stress. However, the **ECI** model does not employ a simplified linear approximation of the interfacial constitutive behavior like the **SIF** model, nor does it introduce additional equations like the **NI** model. The **ECI** model thus combines the simplicity and efficiency of the **FI** and **CCI** models with the physical accuracy of the **NI** and **SIF** models.

The **ECI** model was incorporated into NASA's **MAC/GMC** software package (Arnold et al., 1999), which employs a rate formulation of **GMC**. Thus, like the **CCI** model, a rate form of the interfacial displacement discontinuity equations is employed. The **ECI** model, however, allows the debonding parameters to evolve with time. Thus the equations become,

$$\begin{aligned}
[\dot{u}_n]^I &= R_n(t) \dot{\sigma}_n|^I + \dot{R}_n(t) \sigma_n|^I & \sigma_n|^I &\geq \sigma_{DB}|^I \\
[\dot{u}_t]^I &= R_t(t) \dot{\sigma}_t|^I + \dot{R}_t(t) \sigma_t|^I & \sigma_t|^I &\geq \sigma_{DB}|^I
\end{aligned} \tag{3}$$

Note that, like the **CCI** and **SIF** models, the **ECI** model interface is provided with a finite bond strength. The form of the normal and tangential debonding parameter time-dependence is taken to be,

$$R(t) = \Lambda \left[\exp\left(\frac{\hat{t}}{B}\right) - 1 \right] \quad \hat{t} \geq 0, \tag{4}$$

where Λ and B are empirical constants specific to the interface (to be discussed later), and \hat{t} is the time since debonding. Thus, the debonding parameter is zero (simulating perfect bonding) until the interfacial stress exceeds the interfacial debond stress. At this point, the debonding parameter begins to evolve exponentially with time, eventually becoming large (simulating complete debonding). Recalling that R is, in effect, the compliance of the interface, it is clear that the exponential form of eqn (4) is physically motivated. The compliance starts at zero, and begins to evolve slowly as the interface fails. As time progresses, the degree of debonding increases, and eventually the compliance becomes infinite, simulating an opened interface.

Unlike the interface models discussed previously, the **ECI** model does not provide the explicit constitutive behavior of the interface. That is, one cannot create a plot of the interfacial displacement vs. the interfacial stress simply by using eqn (4); the interfacial response is coupled with the micromechanics solution. This is because the evolution of the debonding parameter, R , affects the global composite response and thus the evolution of all fields in the composite, including the interfacial stress. Consequently, in order to produce a plot of the **ECI** model interfacial constitutive behavior, it is necessary to employ the model in conjunction with **GMC** for a particular composite configuration. Figure 3 shows such a plot for the interface in a 25% SCS-6/TIMETAL 21S composite at 23 °C represented by a 2×2 subcell repeating unit cell (see Section 6 for details) subjected to uniform transverse tension at a strain rate of $4.17 \times 10^{-4} \text{ s}^{-1}$. The following debonding parameters were employed: $\sigma_{DB} = 80 \text{ MPa}$, $B = 4 \text{ s}$, $\Lambda = 5.51 \times 10^{-3} \text{ GPa}^{-1}$. Clearly, from a qualitative standpoint, the **ECI** model agrees well with the physically/statistically motivated **NI** and **SIF** models. The **ECI** model naturally captures the early post-failure behavior embodied by the **SIF** model, while the later interfacial behavior resembles that of the **NI** model. The choice of the exponential form for the debonding parameter, R , is thus substantiated by its similarity to two previous explicit interface models developed based on the physics and statistics of interfacial failure. The **ECI** model surpasses the **SIF** model thanks to its easy and efficient implementation in **GMC** without resorting to a simplified linear approximation (see Fig. 3). Likewise, the **NI** model is eclipsed by the **ECI** model's finite bond strength, the fact that the **ECI** model introduces no additional equations into the micromechanics formulation, and the fact that **GMC**'s closed-form nature is preserved. Most importantly, the **ECI** model provides the ability to more accurately simulate the measured transverse behavior of SiC/Ti composites than the previous interface models discussed.

Despite the similarities between the **ECI** model and other physically/statistically motivated interface models, it may seem more natural to allow the debonding parameter to be a function of a local variable, such as stress at the interface, rather than time (see eqn (4)). However, this actually disallows local stress unloading because the debonding parameter and the local stress both tend to reach a steady-state value. In this condition, the interfacial compliance, R , reaches a value that is sufficiently high to prevent accumulation of additional local stress, which then prevents the debonding parameter from growing larger. Once the debonding parameter stops growing larger, it is a constant and local unloading cannot occur.

The exponential form for the debonding parameters (eqn (4)) was originally chosen because it allows the local stress to unload smoothly, and the parameters Λ and B can be chosen to provide a realistic global response. Other functional forms were examined. A linear form, for instance, did not allow the debonding parameters to evolve sufficiently quickly so as to allow the local stress to unload unless the slope of the linear function was quite high. However, this high slope then caused difficulties due to the rapid initial growth of the debonding parameters. Of the many functional forms that were examined for $R(t)$, the exponential form provided the best combination of features while providing good qualitative agreement with previous interface models. For additional information on the functional form of eqn (4), see Bednarczyk and Arnold (2000).

4. The Generalized Method of Cells (GMC)

The **ECI** model developed to simulate interfacial debonding in composite materials was incorporated into Aboudi's (1991; 1995) **GMC**. The geometry of the doubly periodic version of **GMC** is shown in Fig. 4, wherein the microstructure of a periodic material is represented by a rectangular repeating unit cell consisting of an arbitrary number of rectangular subcells, each of which may be a distinct material. The method assumes a linear displacement field in each subcell and imposes continuity of traction and displacement components between subcells in an average sense (Aboudi, 1995). This procedure results in strain concentration equations, as well as effective thermo-elastoplastic constitutive equations, for an arbitrary periodic material, that are required to simulate the response to external loading.

The recent reformulation of the **GMC** equations (Pindera and Bednarczyk, 1999; Bednarczyk and Pindera, 2000) employs subcell stresses (rather than strains) as basic unknowns and develops mixed concentration equations for the heterogeneous material. Due to **GMC's** *inherent lack of normal-shear field coupling*, significantly fewer unique subcell stress components are present compared to subcell strain components (see Pindera and Bednarczyk (1999) and Bednarczyk and Pindera (2000) for details). Thus the reformulated version of **GMC**, by exploiting the method's lack of shear coupling, now represents an ultra-efficient multi-axial micromechanics analysis tool. Direct comparison of execution times resulting from the reformulated and original versions of **GMC** indicates a striking speed-up associated with the reformulation, particularly as the number of subcells becomes large. For example, for a 12×12 subcell repeating unit cell, the reformulated version of **GMC** has been shown to be more than 19,000 times faster (Bednarczyk and Arnold, 2000). As demonstrated by Pindera and Bednarczyk (1999), the original

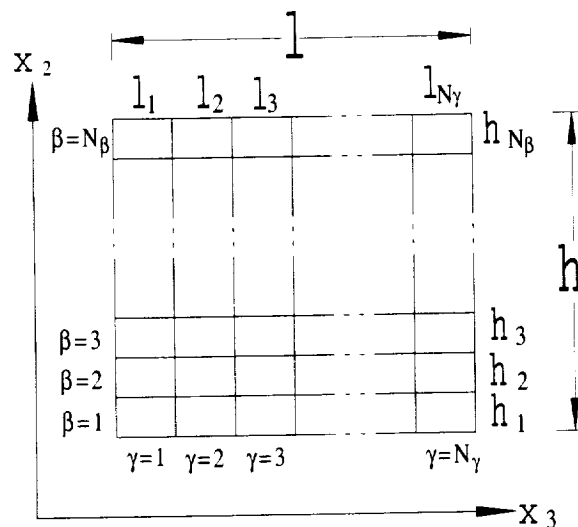


Figure 4: Doubly periodic **GMC** repeating unit cell.

formulation and reformulation of **GMC** yield identical results, thus the speed-up comes with no loss of accuracy. Clearly, utilization of the reformulation is crucial to the realization of reasonable execution times for application of **GMC** to detailed composite microstructures and as an elemental material model within the finite element analysis of structures. In fact, most of the results generated for this study could not have been generated (due to exorbitant execution times) prior to the reformulation of **GMC**.

5. Constituent Materials and Constitutive Models

For this study, the material analyzed is a metal matrix composite composed of continuous silicon carbide fibers (SCS-6) embedded in a titanium alloy matrix, **TIMETAL 21S**. Textron's high-strength, high-stiffness, continuous SiC fibers are assumed in this study to be isotropic and linear elastic. The vendor-supplied temperature-dependent thermoelastic properties employed for the SCS-6 fiber are given by Bednarczyk and Arnold (2000).

TIMETAL 21S is a metastable beta strip titanium alloy, containing approximately 21% alloying additions, that has high strength as well as good creep and oxidation resistance. Consequently, **TIMETAL 21S** has been utilized in advanced metal matrix composites. Its (isotropic) viscoplastic response has been characterized for the Bodner-Partom (**BP**) model (Chan et al., 1988; Chan and Lindholm, 1990) by Neu (1993) and Kroupa (1993), as well as for a generalized viscoplasticity with potential structure (**GVIPS**) model (Arnold and Saleeb, 1994) by Arnold et al. (1996b;c). Both the **BP** and the **GVIPS** models have been employed in the current study.

The reader is referred to Arnold et al. (1996b;c) for the development of the **GVIPS** equations, as well as material parameters and the associated parameter interpolation functions (employed to determine the material parameters for **TIMETAL 21S** at temperatures other than the reference temperature of 650 °C). Similar information for the **BP** model is available in Neu (1993) and Kroupa (1993).

6. ECI Model Application

6.1 General Features

In order to gain further insight into the character of the **ECI** model, consider the **MAC/GMC** repeating unit cell shown in Fig. 5. This is the simplest doubly periodic unit cell that may be used to represent a unidirectional continuously reinforced composite. It consists of one fiber subcell surrounded by three matrix subcells, and it is infinitely long in the out-of-plane direction. Note that the unit cell repeats infinitely in the two in-plane directions. A simple application of the new debonding model involves placing an interface between the fiber and matrix as shown in Fig. 5 and applying simulated

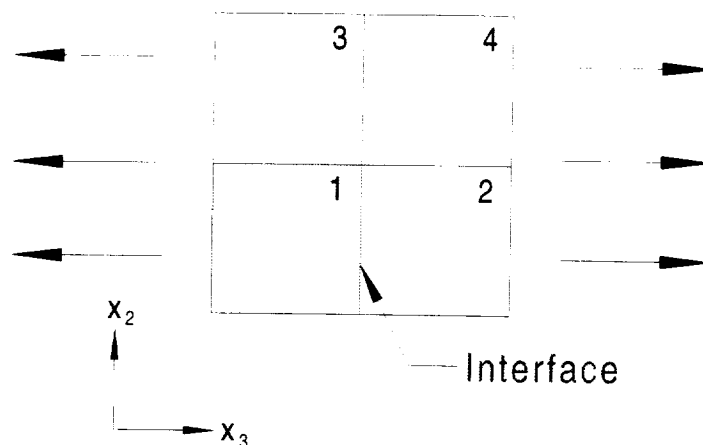


Figure 5: Simple 2x2 composite unit cell for simulating transverse debonding at an interface.

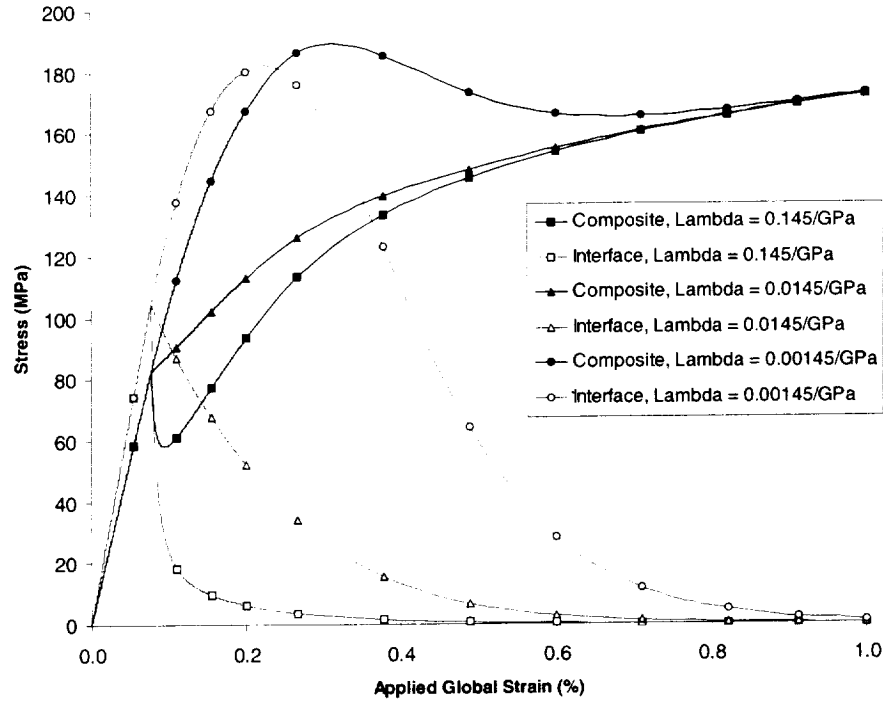


Figure 6: Effect of Λ on the predicted local and global transverse tensile behavior of a 20% SCS-6/TIMETAL 21S composite at 650 °C. $\dot{\epsilon} = 1.11 \times 10^{-4} \text{ s}^{-1}$.

transverse tension. The results for this example are displayed in Fig. 6, where a 20% SCS-6/TIMETAL 21S composite (at 650 °C) has been modeled. The predicted global (composite) stress and the local interfacial stress (in the loading direction) are plotted versus the applied global strain (*not* the interfacial displacement) for different values of the debonding parameter Λ (see eqn (4)). The value of B was fixed at 10. s, although a similar plot could be generated by fixing the value of Λ and varying the value of B . A σ_{DB} value of 103 MPa was employed. Note that residual stresses have not been included for this simple example.

Clearly the interfacial behavior (which is determined by the choice of Λ , B , and σ_{DB}) has a major impact on the predicted composite transverse tensile behavior. If the interface is permitted to unload too quickly (high Λ value or low B value), the predicted global stress-strain curve will exhibit an unrealistic “dip” upon debonding. Conversely, if the interface is permitted to unload too slowly (low Λ value or high B value), the global stress strain curve will exhibit an unrealistic “hump” while unloading is occurring. A similar unrealistic “hump” is typical to simulations performed using the NI model (McGee and Herakovich, 1992; Eggleston, 1993). Note that all three predicted global (composite) stress-strain curves in Fig. 6 converge once the interfacial stress becomes small, a direct result of the lack of shear coupling inherent to GMC. GMC’s lack of shear coupling causes constancy of certain stress components in certain directions. Recall, however, that it is precisely this characteristic that permits the reformulation of the GMC equations for increased computational efficiency. Referring to Fig. 5, the normal stress component in each direction is constant in rows of subcells in the appropriate direction. That is,

$$\begin{aligned}
\sigma_{33}^{(1)} &= \sigma_{33}^{(2)} \\
\sigma_{33}^{(3)} &= \sigma_{33}^{(4)} \\
\sigma_{22}^{(1)} &= \sigma_{22}^{(3)} \\
\sigma_{22}^{(2)} &= \sigma_{22}^{(4)}
\end{aligned} \tag{5}$$

where the superscripts correspond to the subcell numbers shown in Fig. 5. Thus, when the interface shown in Fig. 5 debonds and the “interfacial” stress (in the x_3 -direction) unloads, σ_{33} in the entire row of subcells (subcells #1 and #2) unloads. Then, when this stress component becomes sufficiently small, the repeating unit cell is left with only subcells #3 and #4 to carry the applied loading. Hence, once the “interfacial” stress unloads completely, the predicted composite response will be identical for different simulations regardless of the values of Λ and B . Further, the curve to which the simulations converge is dictated by the fraction of the composite cross-section that remains intact to carry the applied loading (i.e., the x_2 dimension of subcells #3 and #4). For a given fiber shape in the **GMC** repeating unit cell, this remaining intact area can be related to the fiber volume fraction of the simulated composite.

It is interesting to note that, due to the aforementioned “dip” and “hump” exhibited by two of the global (composite) stress-strain curves shown in Fig. 6, it is possible to determine a range of realistic values for Λ and B for a given material system, repeating unit cell, and set of loading conditions *with no knowledge of the actual composite response*. That is, a reasonable set of parameters for the debonding model can be chosen simply based on physicality (i.e., no “dips” or “humps” in the predicted response). As will be shown, however, characterization of the model using certain experimental data will render the simulations much more realistic than those that can be obtained simply by requiring the predictions to appear realistic from a qualitative standpoint.

6.2 Effect of Debonding Event Cross-Section

The fact that the appropriate stress component in an entire row of subcells unloads upon interfacial failure also gives rise to a debonding event cross-section influence on the composite response. Consider the repeating unit cell shown in Fig. 7. It has the same fiber volume fraction as the unit cell shown in Fig. 5, however, the effective fiber cross-section (in the loading direction) is vastly different. Transverse tensile predictions for the 20% SCS-6/TIMETAL 21S composite (at 650 °C) examined previously are shown in Fig. 8, where the two unit cells shown Figs. 5 and 7 have been used. The fiber shape (square or rectangular) has a minor effect on the predicted global response for perfect bonding.

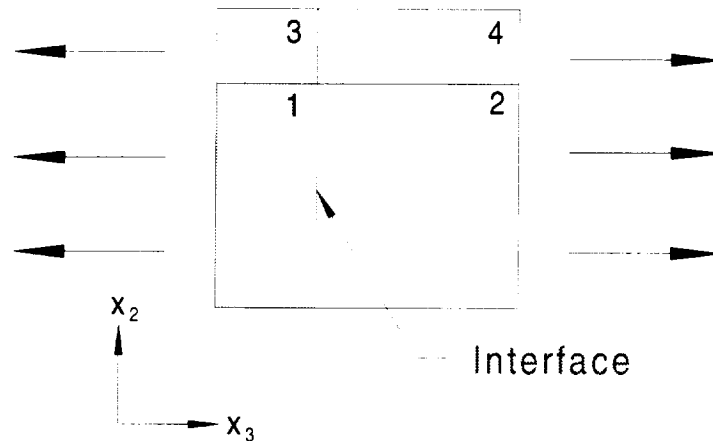


Figure 7: Another simple repeating unit cell for transverse debonding.

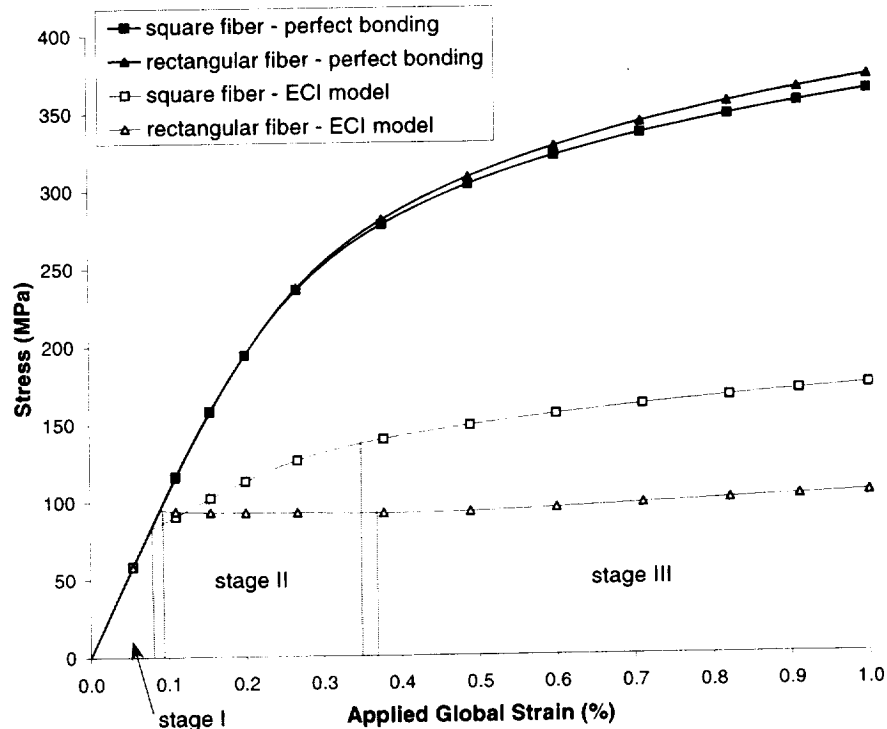


Figure 8: Effect of debonding event cross-section on the predicted transverse tensile behavior of a 20% SCS-6/TIMETAL 21S composite at 650 °C. $\dot{\epsilon} = 1.11 \times 10^{-4} \text{ s}^{-1}$.

However, when the **ECI** model is employed, the difference caused by the difference in fiber shape is extreme. Since a much larger cross-section of the repeating unit cell is associated with the debonding event in the case of the rectangular fiber, the event has a more drastic effect on the composite response immediately after debonding. As stated previously, this effect is an artifact of **GMC**'s lack of shear coupling. Clearly, the qualitative character of the stage II global composite behavior should not change so drastically as that shown in Fig. 8 simply as a result of changing the fiber shape. Thus, in employing the **ECI** model across composite configurations with different failure event cross-sections (e.g., different interface sizes), the **ECI** model parameters, Λ and B , should be altered to minimize the effects of this artifact. It should be noted that for fibers with identical shapes and subcell grid discretizations, as the fiber volume fraction increases, so does the percentage of the unit cell cross-section associated with each failure event. It is thus possible to adjust the debonding parameters for different fiber volume fractions to minimize the effects of the aforementioned artifact.

A second effect of changing the fiber shape is also evident in Fig. 8; the final stage III stress that is reached (at an applied strain of 1.0 %) by the composite with the rectangular fiber is significantly lower than that reached by the square fiber. As mentioned previously, this effect is due to differences in the size of the remaining intact region of the composite after debonding. In the case of the rectangular fiber, a much smaller matrix ligament remains intact after the interface has debonded and unloaded. The composite can then support much less stress for a given global strain level. Unlike the stage II effect of the failure event cross-section, the stage III effect is *not* an artifact. Clearly, if a greater percentage of the composite debonds, the stress that the composite can support at a given global strain level should be reduced. Thus it is not necessary to compensate for this effect. However, this effect can be used as an aid when calibrating the **ECI** model and the extent of permitted debonding for a particular simulation.

Suppose (for example) that we wish to employ the **ECI** model in conjunction with a **GMC** repeating unit cell like that shown in Fig. 5 to simulate the transverse tensile response of a particular SCS-6/TIMETAL 21S composite for which experimental data is available. Previous work has shown that the

entire fiber cross-section (as indicated in Fig. 5) does not debond during transverse tension. Rather, debonding progresses to a certain point (at which the radial interfacial stress becomes compressive) and then, as final composite failure initiates, a crack propagates through the matrix to adjacent fibers (Karlak et al., 1974; Nimmer et al., 1991; Hu, 1996). One might model the partial debonding phenomenon as shown in Fig. 9, where only part of the fiber-matrix interface is modeled as weak, and the remaining portion of the interface (over a length δ) is treated as strongly bonded. The ratio of the intact bond length δ to the fiber dimension d can then be selected such that the stress reaches a desired level at 1% strain (for instance). Figure 10 shows an example of transverse tensile simulations in which the desired stress at 1% strain was 200 MPa. Allowing the entire interface to debond resulted in a stress at 1% strain of 172 MPa. By adjusting the ratio of δ/d to 16%, the desired composite stress of 200 MPa at 1% global strain was achieved. Note that a bond strength of zero was used in the above example. The bond strength value does not matter as long as the interfacial stress completely unloads by the time the desired strain level, 1% in the example, is reached. Once the desired stress level is achieved as described in the example, the remaining ECI model parameters, σ_{DB} , Λ , and B , may be chosen to provide good correlation with the experimental response.

6.3 Effect of Strain Rate

Another influence that is felt by the ECI model is that of global loading rate. Since the evolution rates of R_n and R_r are explicit functions of time (see eqn (4)), the time-dependent behavior of a particular interface will be identical regardless of the global loading rate. That is, for example, if the simple repeating unit cell shown in Fig. 5 is subjected to simulated transverse strain at a high strain rate and a low strain rate using identical values for Λ and B , the interface will respond over the same amount of time in both cases. Since the global strain rates are different, the global strain at a particular point in time will be different between the two cases, and the predicted global stress-strain response of the composite will be vastly different. This is illustrated in Fig. 11, which shows the predicted response for the same 20% SCS-6/TIMETAL 21S composite (at 650 °C) examined previously for three different applied strain rates. It is clear that the unloading behavior of the interface appears different among the three cases. For the high applied global strain rate, the interface does not have sufficient time to unload, while for the low applied global strain rate, the interface unloads completely at a relatively low applied global strain. The interfacial behavior has a major impact on the predicted global composite behavior as well. From Fig. 11 it is clear that the applied strain rate effect is an artifact of the explicit time dependence of the interfacial compliance in the ECI model. The overall character of the stage II composite response should not change

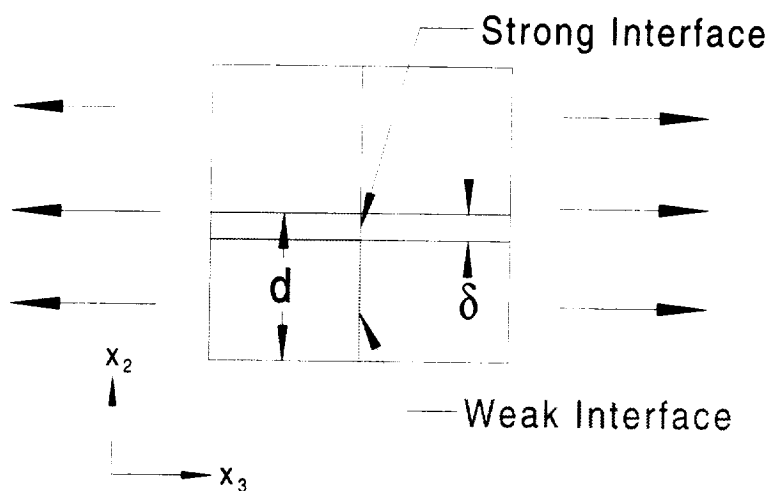


Figure 9: GMC repeating unit cell for simulating incomplete fiber-matrix debonding.

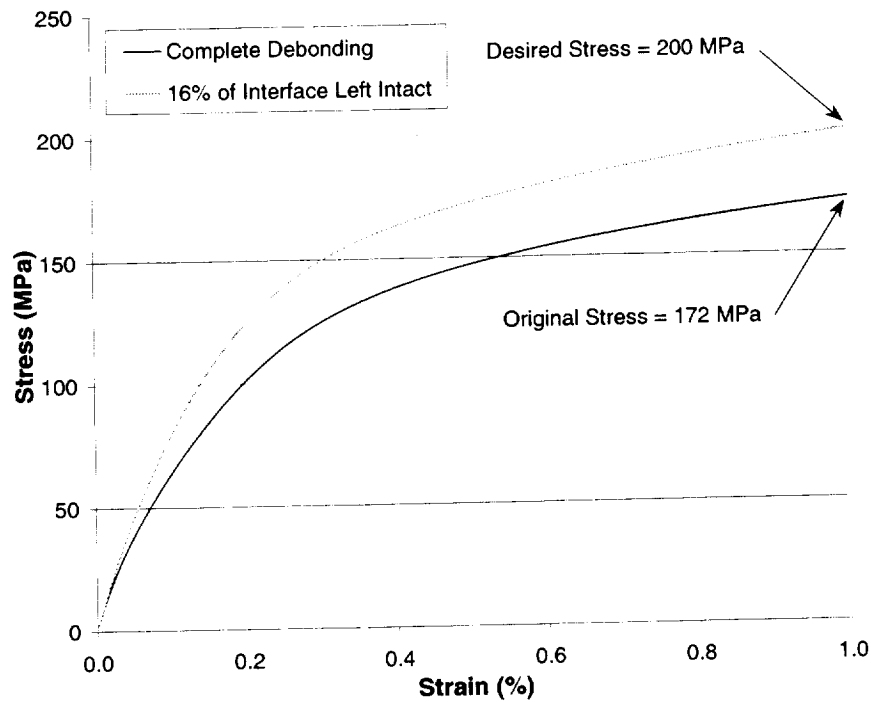


Figure 10: Simulated transverse tensile response of 20% SCS-6/TIMETAL 21S at 650 °C with zero interfacial bond strength over a portion of the fiber-matrix interface used to select a desired stress at 1% strain. $\dot{\epsilon} = 1.11 \times 10^{-4} \text{ s}^{-1}$.

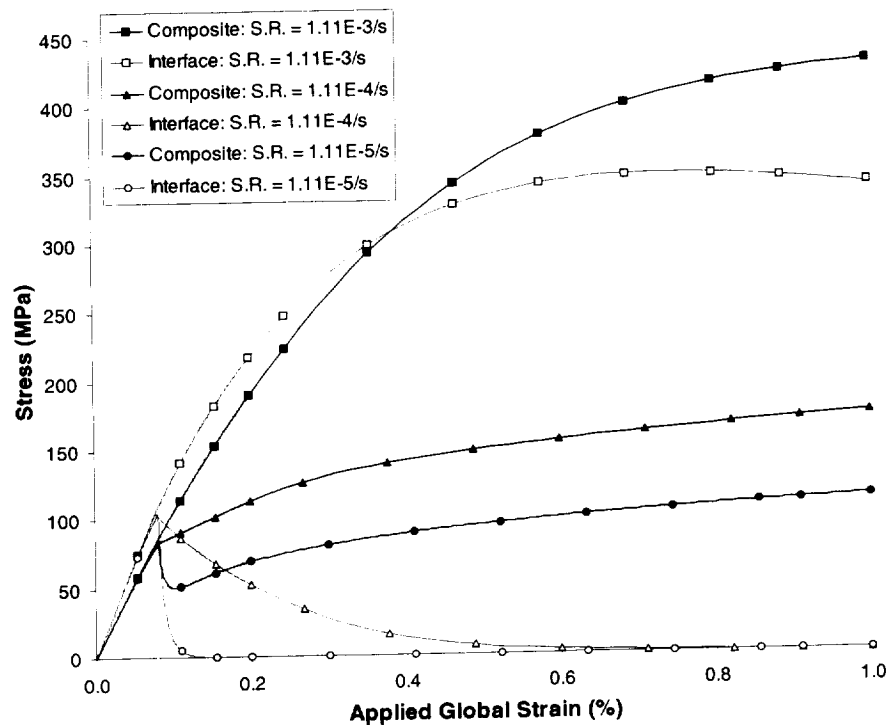


Figure 11: Effect of applied global strain rate (S.R.) on the predicted transverse tensile behavior of a 20% SCS-6/TIMETAL 21S composite at 650 °C.

drastically based on strain rate. Fortunately, the **ECI** model can easily be corrected for this artifact via alteration of the parameter B , according to the equation,

$$B = B_{\text{ref}} \left(\frac{\dot{\bar{\epsilon}}_{\text{ref}}}{\dot{\bar{\epsilon}}} \right). \quad (6)$$

As discussed by Bednarczyk and Arnold (2000), since the parameter B scales the time dependence in the **ECI** model (see eqn (4)), it is possible to determine empirically a B_{ref} value based on correlation with experiment at a particular global strain rate, $\dot{\bar{\epsilon}}_{\text{ref}}$, and simply scale the parameter B , via eqn (6). It should be noted that the applied global strain rate also affects the predicted composite behavior independently from the interfacial behavior through the strain rate dependence of the matrix viscoplastic constitutive model. This explains the non-convergence of the composite curves for the lower two strain rates despite the fact that the interfaces completely unloads its stress in these cases. Obviously, this influence of strain rate is not an artifact and should not be compensated for.

6.4 Effect of Debonding Model

Figure 12 compares model predictions for the same 20% SCS-6/TIMETAL 21S composite (at 650 °C) examined previously, where three different interfacial bonding conditions have been simulated: perfect bonding, debonding via the **CCI** model (see section 3.2), and debonding via the **ECI** model. By employing the **CCI** model rather than perfect bonding, a significant decrease in the overall predicted composite stiffness results. As described in Section 3.2, the interfacial stress becomes constant in the case of the **CCI** model once debonding has occurred. By employing the **ECI** model, which allows the interface to unload, a further reduction in the overall predicted composite stiffness is realized, which, as will be shown, allows improved accuracy when simulating the composite response.

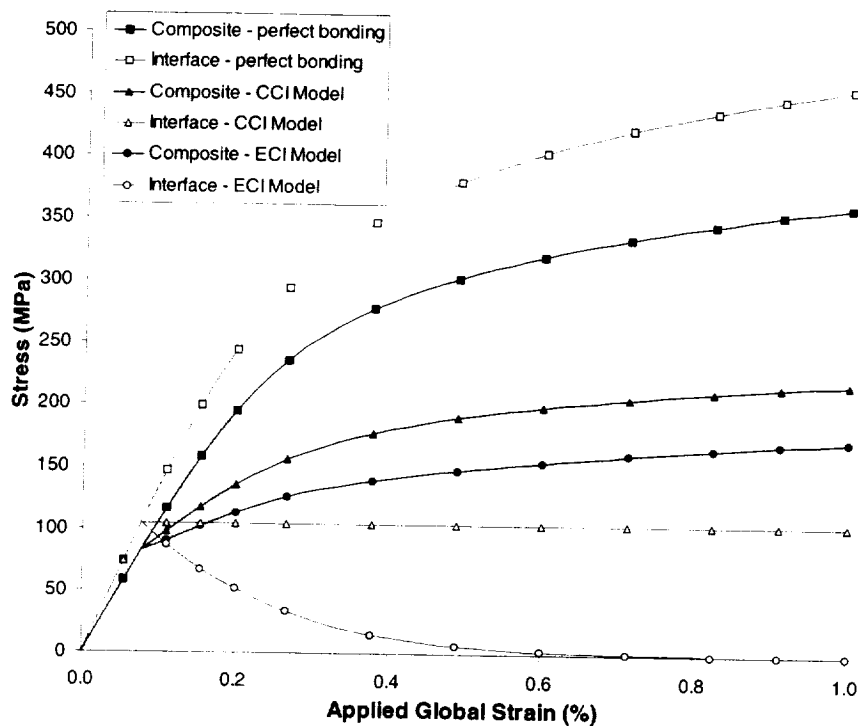


Figure 12: Comparison of the predicted local and global transverse response of a 20% SCS-6/TIMETAL 21S composite at 650 °C using different interfacial debonding models. $\dot{\bar{\epsilon}} = 1.11 \times 10^{-4} \text{ s}^{-1}$.

6.5 Effect of Matrix Constitutive Model

One final effect that has a significant impact on the global manifestations of the debonding model is the matrix inelastic constitutive model. The **MAC/GMC** predictions shown thus far have all employed the **GVIPS** viscoplastic constitutive model for the **TIMETAL 21S** matrix (Arnold et al., 1996b;c). An alternative Bodner-Partom (**BP**) viscoplastic constitutive model is available for **TIMETAL 21S** (Neu, 1993; Kroupa, 1993). As will be shown, if this particular **BP** model is employed for the matrix, the transverse tensile predictions for the composite can be quite different. The elevated temperature tensile constitutive behavior of **TIMETAL 21S**, as simulated using the **GVIPS** model and this **BP** constitutive model, is compared with experimental data in Fig. 13. Both models tend to overpredict the matrix response at this temperature and strain rate. Early on, **GVIPS** exhibits better agreement with experiment, while at the higher strains, **BP** provides the more realistic prediction. For the case plotted, **GVIPS** overpredicts the experimental stress at 1.9% strain by 16.7%.

Figure 14 compares experimental creep data for **TIMETAL 21S** with model predictions for both **GVIPS** and **BP** at 650 °C with different applied stress levels. While **GVIPS** tends to underpredict the magnitude of the creep strain, especially as the time becomes large, it is significantly more realistic than the **BP** model employed herein in that a primary creep regime exists with the **GVIPS** model. Alternatively, the **BP** model predicts immediate steady-state creep; it significantly underpredicts the creep at low applied stress levels and drastically overpredicts the creep at higher applied stress levels. As will be shown, these characteristics of the simulated matrix response brought about by the choice of constitutive model carry over to the transverse response of the composite. It is also important to keep in mind that, as discussed by Nimmer et al. (1991), the time-dependent constitutive model response affects the residual interfacial clamping stress in simulations of the composite response. This, in turn, can have a major impact on the simulated debonding in the composite.

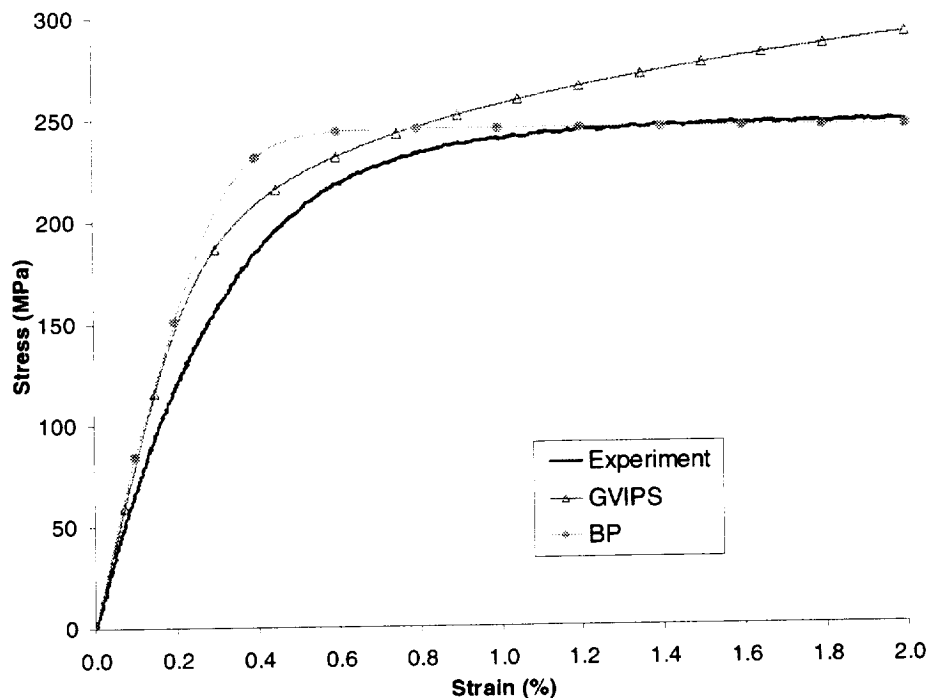


Figure 13: Comparison of matrix constitutive models for the tensile response of **TIMETAL 21S** at 650 °C for $\dot{\epsilon} = 1 \times 10^{-4} \text{ s}^{-1}$.

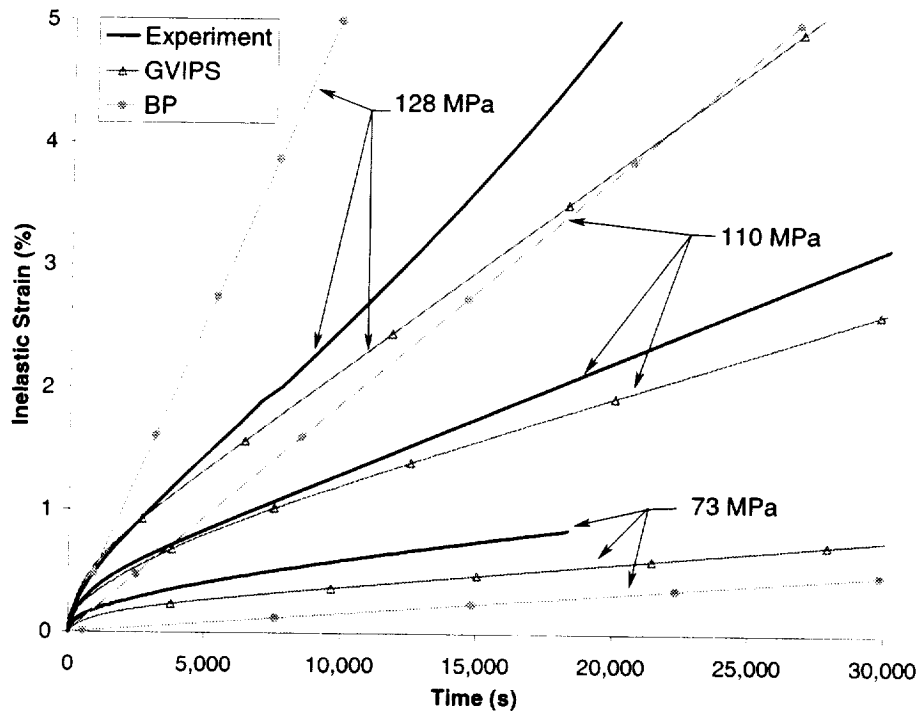


Figure 14: Predicted and experimental creep behavior of TIMETAL 21S at 650 °C.

7. Results and Discussion

7.1 Transverse Tension

The actual model simulations for transverse tension employ a more complex (and realistic) geometric representation for the composite than the one presented previously (see Fig. 5). A photomicrograph of an actual SCS-6/TIMETAL 21S composite cross-section is shown in Fig. 15. The composite has layers of pure matrix on both the top and bottom, and the packing of the fibers in the region between the pure matrix layers is rectangular rather than square. Microstructural features such as these generally do not have a significant impact on the longitudinal behavior of continuous composites, but the effects of these features on the transverse behavior of composites can be quite pronounced (Arnold et al., 1996a; Bowman, 1999; Goldberg and Arnold, 2000). The **MAC/GMC** representation for the composite is shown in Fig. 16; wherein the laminate theory capabilities of **MAC/GMC** (see Arnold et al. (1999) for details) were employed to model the composite as a laminated plate with three layers. **MAC/GMC** employs a multi-scale approach that allows each layer of the laminate to be a monolithic material or a unidirectional composite whose behavior is modeled with **GMC**. Thus, the viscoplastic constitutive models and debonding models available in **MAC/GMC** may be applied to the composite material contained within a particular layer of the laminate. The (normalized) thickness of each layer is indicated in Fig. 16. Furthermore, a well-refined circular representation of the fiber (26×26 idealization containing 676 subcells) was employed. Thanks to the recently implemented reformulated version of **GMC** within **MAC/GMC**, the execution of such a large problem was still rapid. Finally, the measured average aspect ratio (width divided by height of the unit cell, as drawn in Fig. 16, denoted as R) of the core region of the composite was employed (i.e., $R=0.82$), as was the proper local fiber volume fraction ($V_f = 0.273$) required to yield the measured overall fiber volume fraction of 20%.

Previously, the **ECI** model was used by Bednarczyk and Arnold (2000) to simulate the longitudinal failure behavior of TMCs. In that study, a simulated interface was placed within each continuous fiber, normal to the fiber direction. Then, debonding of a particular simulated interface was

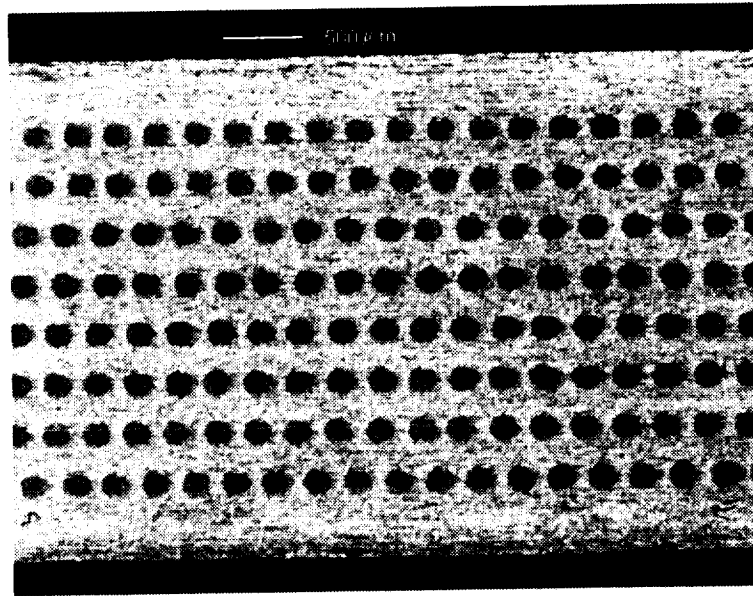


Figure 15: Photomicrograph of the cross-section of a 20% SCS-6/TIMETAL 21S composite. Courtesy of C.L. Bowman.

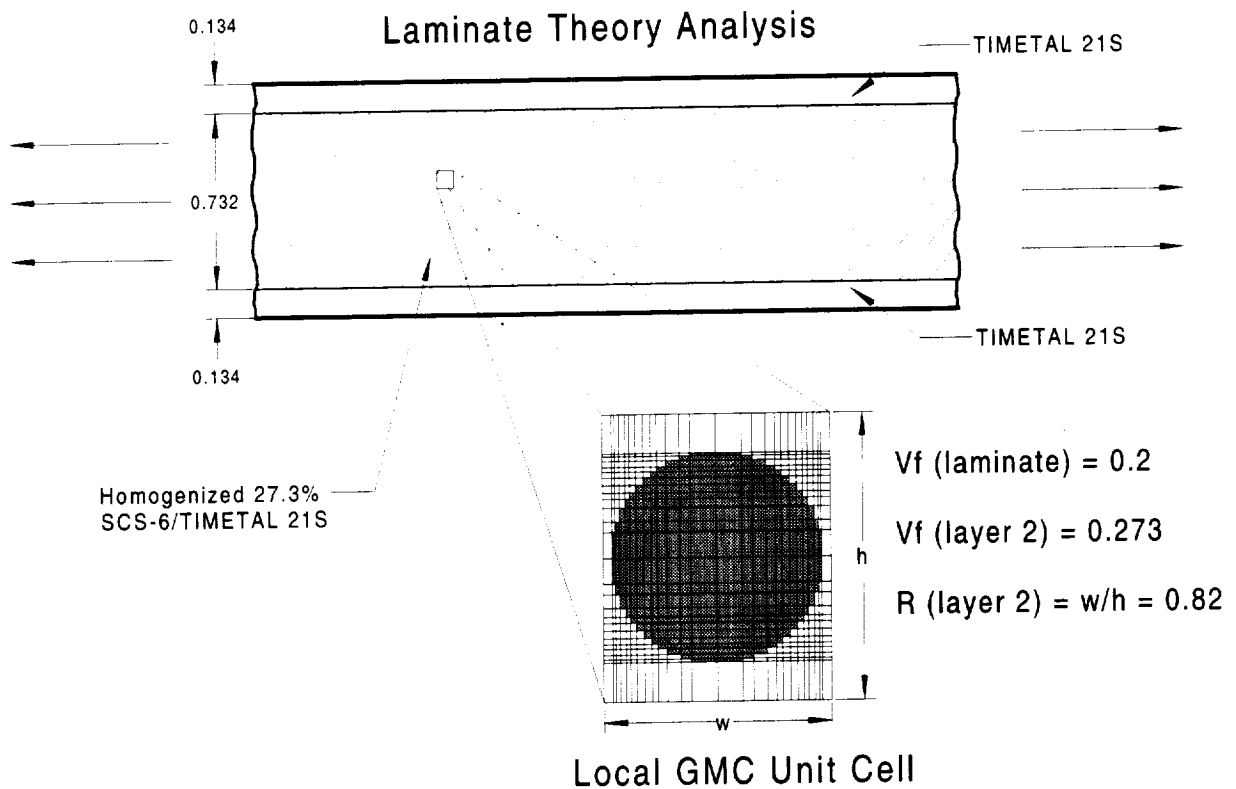


Figure 16: MAC/GMC representation of the SCS-6/TIMETAL 21S composite.

used to simulate failure of the fiber in which the interface was placed. The bond strength of each interface, which represented the strength of each fiber, could thus be taken from measured fiber strength histograms. Analogous data is unavailable for the fiber-matrix interfacial bond strengths in TMCs, thus these strengths, along with the parameters A and B, must be selected based on correlation with experimental data.

The simulated bond strengths associated with each fiber-matrix interface in the **GMC** repeating unit cell (determined using the **GVIPS TIMETAL 21S** constitutive model in **MAC/GMC**) are shown in Fig. 17. Note that debonding perpendicular to the loading direction was disallowed as it was observed to have no noticeable effect on the transverse tensile behavior. Although only one quarter of the unit cell is pictured because the bond strengths are the same (in the loading direction) for each quadrant, this does not imply that only one quarter of the repeating unit cell is analyzed (as is often the case when employing finite element analysis). In **GMC**, symmetry conditions are not employed; the entire unit cell is analyzed as, depicted in Fig. 16.

The experimental stress-strain curve used to characterize the interfacial bond strengths, as well as the parameters A and B, is shown in Fig. 18. The resulting simulated stress-strain curve with the three characteristic stages of the deformation behavior of the composite identified by Majumdar and Newaz (1992) is shown as well. Note that residual stresses from fabrication were incorporated in the simulations via a stress-free cool down from elevated temperature prior to application of the simulated heat-up to 650 °C, which was followed by the simulated tensile loading. However, because 650 °C is close to the composite processing temperature, these residual stresses are low (see Fig. 19 for sample interfacial residual stresses). From Fig. 18 it is clear that the model does a reasonably good job of reproducing the experimental response, however the model tends to overpredict the tensile stress of the composite somewhat (by 17.6% at the point of global load reversal, 1.9% strain).

When evaluating the agreement between the **MAC/GMC** simulation and experiment in Fig. 18, the accuracy of the simulated response of the matrix constituent shown in Fig. 13 should be kept in mind. That is, the stage II and III discrepancy between simulation and experiment in Fig. 18 is similar to the

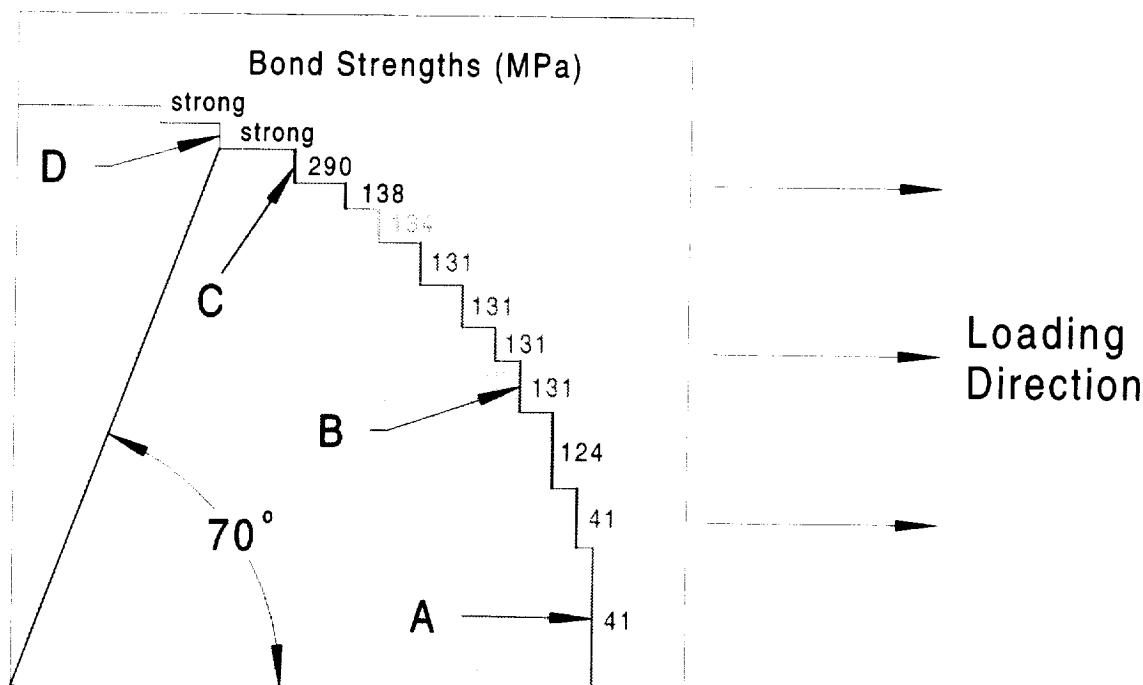


Figure 17: Interfacial bond strengths used for simulations with the **GVIPS** matrix constitutive model in **MAC/GMC**.

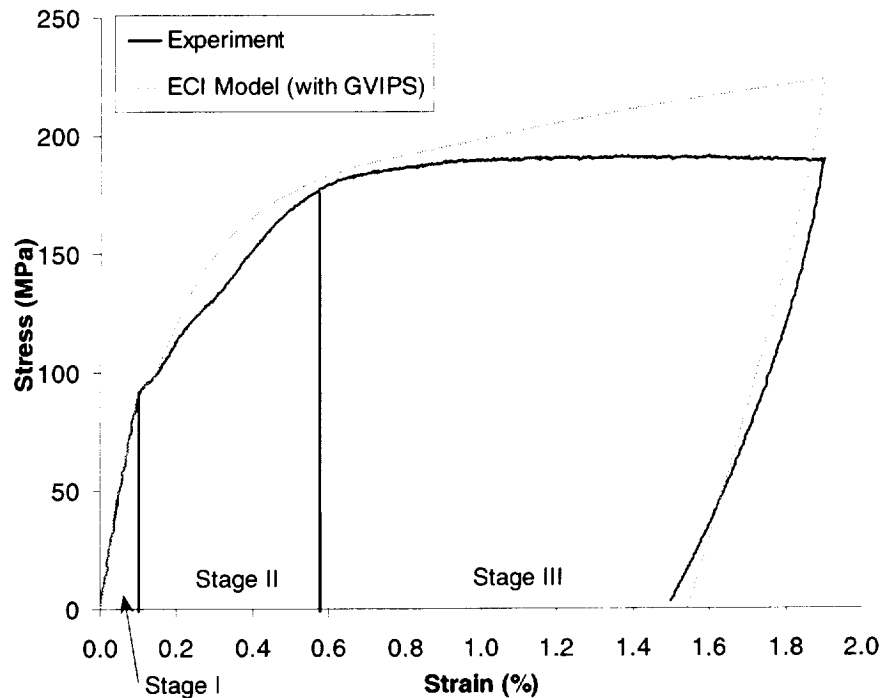


Figure 18: Simulated and experimental transverse tensile response of 20% SCS-6/TIMETAL 21S at 650 °C - debond model parameter characterization. $\dot{\epsilon} = 10^{-4} \text{ s}^{-1}$.

discrepancy between the **GVIPS** constitutive model simulation and experiment in Fig. 13 for the monolithic matrix material. Recall that for the monolithic Ti matrix, the **GVIPS** model overpredicted the tensile stress by 16.7% at a strain of 1.9%. The discrepancy thus should not necessarily be attributed to a deficiency in the **ECI** debonding model. In fact, it would be inappropriate to attempt to compensate for the inaccuracies caused by the matrix constitutive model via a recalibration of the debonding model parameters, even though such compensation could easily be made. It is clear that, as discussed previously, accurate material constitutive characterization is critical to obtain the most realistic simulation of the transverse behavior of TMCs possible.

Revisiting Fig. 17, it is important to observe that the simulated interfacial debond strengths increase as θ increases, that is, as one moves from the lower right ($\theta=0^\circ$) to the upper left ($\theta=90^\circ$). The selection of this trend was motivated by geometric considerations; that is, the need to blend in a consistent manner Cartesian and cylindrical coordinate systems. In particular, the **GMC** idealization is comprised of a number of rectangular shaped subcells, for which all fiber-matrix interfaces are normal (or transverse) to the loading direction. However, the outward normal to the actual fiber-matrix interface, since the interface is curved, becomes increasingly normal to the loading direction as θ increases. Thus the component of the local stress vector that is actually normal to the interface should decrease as θ increases, but this cannot occur in the **GMC** unit cell representation. In **GMC**, the two in-plane normal stress components are always normal or transverse to the interfaces, and no shear stress is present. To overcome this difficulty, the interfacial debond strength of the simulated interface is increased as θ increases from 0° to 90° . This also allows the portion of the interface that is in reality most normal to the loading to debond first, while the remaining interfaces “unzip” in succession. The final two interfaces are treated as strong, meaning they are not permitted to debond. This is motivated mainly by correlation with experiment. Recall that the transverse response of the composite is greatly influenced by the fraction of the cross-section that debonds (see Figs. 9 and 10). If either of these final two interfaces were permitted to debond and unload, the predicted stress-strain curve would be unrealistically low compared to the

experimental stress-strain curve in Fig. 18. As discussed earlier, previous work on debonding in MMCs (Karlak et al., 1974; Nimmer et al., 1991; Hu, 1996) has indicated that, in transverse tension, fiber-matrix interfacial debonding progresses only to a certain angle, at which point the radial stress at the interface becomes compressive. Further debonding or crack propagation through the matrix to the fibers above and below would then occur immediately prior to global failure of the composite. As shown in Fig. 17, by disallowing debonding of the final two interfaces, **MAC/GMC** indicates a 70° debonding zone. The tensile failure behavior of the composite, which may involve further debonding and matrix cracking, is not addressed in this study.

Based on the correlation shown in Fig. 18, the value of **B** was given a constant value of 10 s. Similarly, the value of **A** was given a value of 5.8 GPa⁻¹ for all interfaces except interface “C” (as labeled in Fig. 17). Due to the high debond strength of this interface, a smaller value of **A** (0.725 GPa⁻¹) was required in order to provide the best correlation with the experimental data. Also, note that the unloading behavior of the composite has been modeled reasonably well in Fig. 18. Since the predicted interfacial stress has almost completely unloaded by the time of the load reversal, the interface “closes” almost immediately. That is, as a feature of the **ECI** model, as soon as the stress at a debonded interface becomes compressive, the model treats the interface as perfectly bonded. As Fig. 18 illustrates, this mechanism appears to be reasonably realistic. If at some point in the future a previously debonded interface experiences tensile stress once again (i.e., the composite is reloaded in tension), the interface debonds immediately as any prior chemical bond has been broken and thus the interface can support no tensile stress. Full characterization of the **ECI** model for cyclic application is the subject of future work. As indicated by Nimmer et al. (1991), McGee and Herakovich (1992), and Robertson and Mall (1994), accurate simulation of the transverse cyclic tensile behavior of TMCs, especially when unloading occurs in stage II of the deformation response, is complex and worthy of study in its own right.

Fig. 19 shows the simulated global stress-strain response of the composite as well as the local stress (in the loading direction) versus the applied global strain at the four fiber-matrix subcell interfaces, labeled A,B,C and D in Fig. 17. The utility of enabling progressive debonding around the fiber-matrix interface via different interfacial bond strengths is clear as the realistic knee in the global stress-strain response (see also Fig. 18) is well modeled. Alternatively, if the **CCI** model (see Section 3.2) is employed (using the same debond strength distribution, Fig. 17), the simulated local and global response shown in Fig. 20 is obtained. Clearly, due to the fact that, after debonding, the interfacial debonding cannot progress and the interfacial stress cannot unload, the knee of the global stress-strain curve is not well modeled, and the overall predicted global response is stiffer.

Figure 21 compares three simulations for the transverse tensile response of 20% SCS-6/TIMETAL 21S at 650 °C made using the **ECI** and **CCI** debonding models, as well as a simulation made assuming perfect interfacial bonding, with experimental tensile data. Figure 22 shows a detail of Stages I and II of the response. The figures indicate that as the interfacial behavior modeling is progressively refined, i.e., from perfect bond to weak bond with no unloading (**CCI** model) to weak bonding with unloading (**ECI** model) the simulated results progressively improve as compared with experiments. Note the exceptional ability of the **ECI** model reproduce the experimental data for the characteristic knee evident in Fig. 22 (recall that the **ECI** model parameters were characterized based on the experimental data shown).

To further illustrate the importance of the matrix constitutive model, results for the transverse tensile response of 20% SCS-6/TIMETAL 21S at 650 °C were also generated using the **BP** constitutive model for the TIMETAL 21S matrix. These results are compared with **GVIPS** predictions and experimental tensile data in Fig. 23. As discussed in Section 6.5, the choice of matrix constitutive model has a major impact on the simulated transverse composite behavior not only through the overt representation of the inelastic behavior but also through the residual interfacial clamping stress. Consequently, to allow realistic simulations using the **BP** matrix constitutive model, the debonding model parameters must be altered. The new distribution of interfacial debond strengths for use with the **BP** model are given in Fig. 24. It was not necessary to alter **A** or **B**.

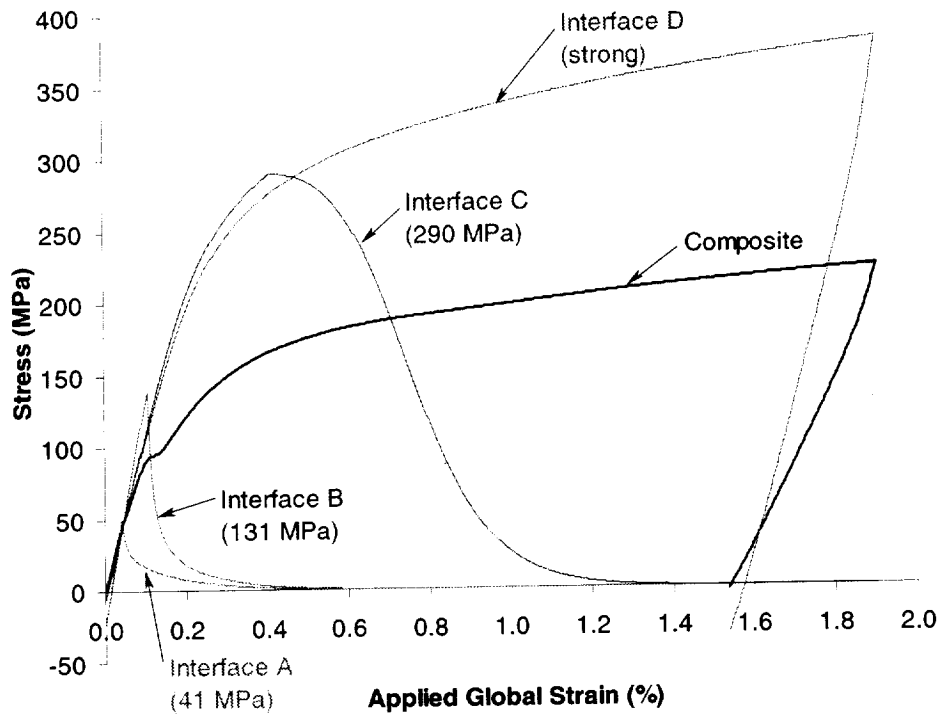


Figure 19: Simulated local and global transverse tensile response of 20% SCS-6/TIMETAL 21S at 650 °C. GVIPS matrix constitutive model and new debonding model were employed. $\dot{\epsilon} = 10^{-4} \text{ s}^{-1}$.

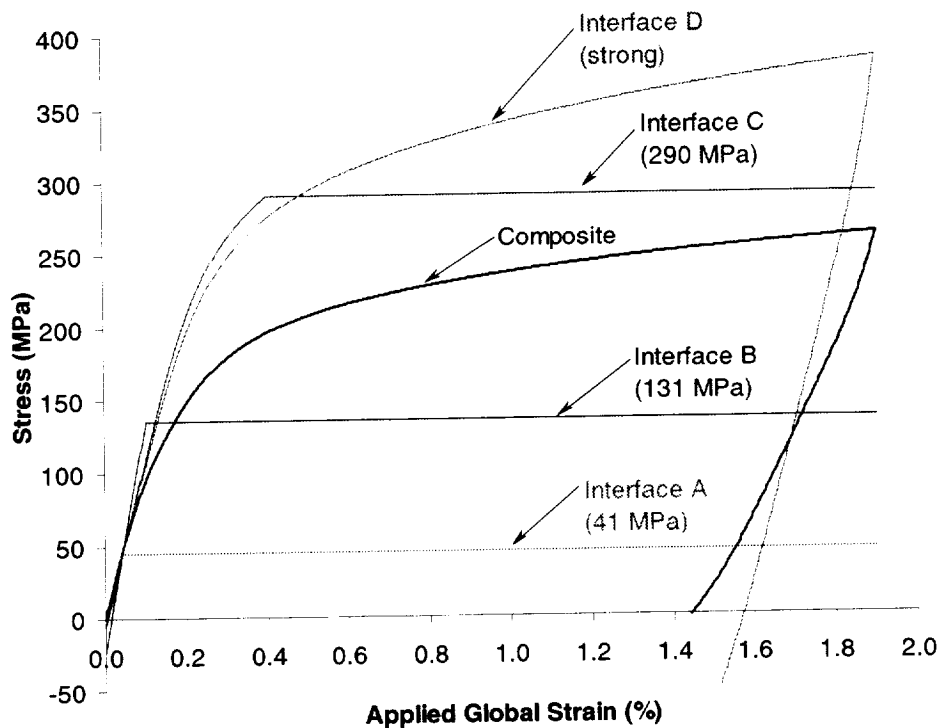


Figure 20: Predicted local and global transverse tensile response of 20% SCS-6/TIMETAL 21S at 650 °C. GVIPS matrix constitutive model and former debonding model were employed. $\dot{\epsilon} = 10^{-4} \text{ s}^{-1}$.

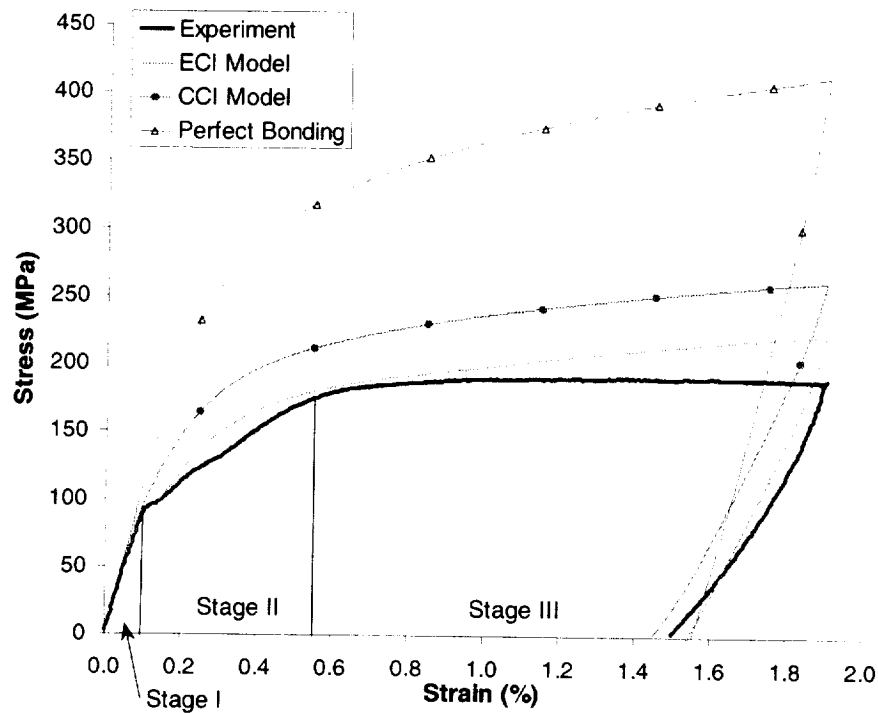


Figure 21: Predicted and experimental response of 20% SCS-6 TIMETAL 21S at 650 °C. The effect of debonding model is highlighted. The **GVIPS** matrix constitutive model was employed. $\dot{\epsilon} = 10^{-4} \text{ s}^{-1}$.

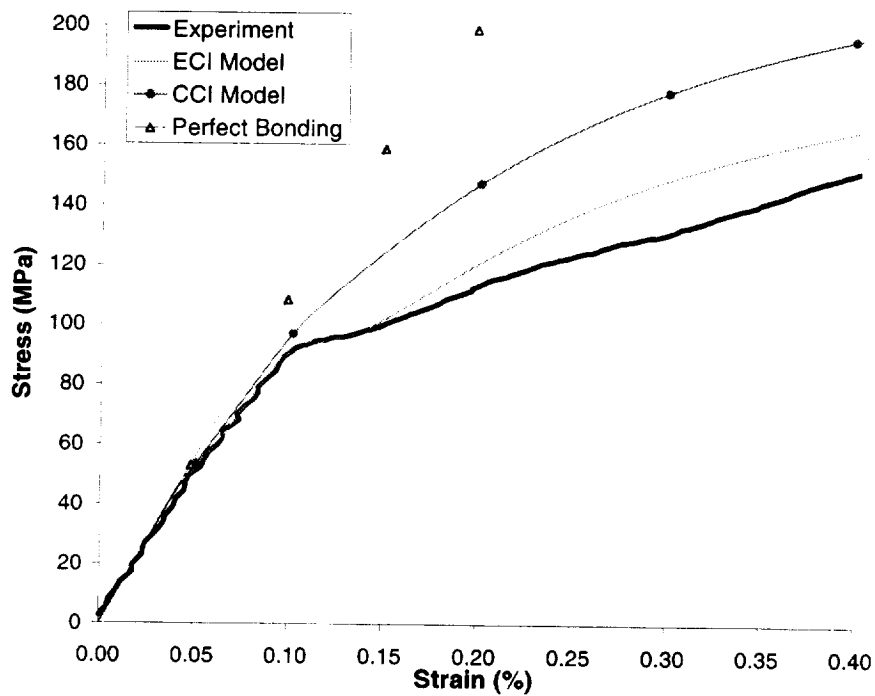


Figure 22: Detail of the predicted and experimental response of 20% SCS-6 TIMETAL 21S at 650 °C. The effect of debonding model is highlighted. The **GVIPS** matrix constitutive model was employed. $\dot{\epsilon} = 10^{-4} \text{ s}^{-1}$.

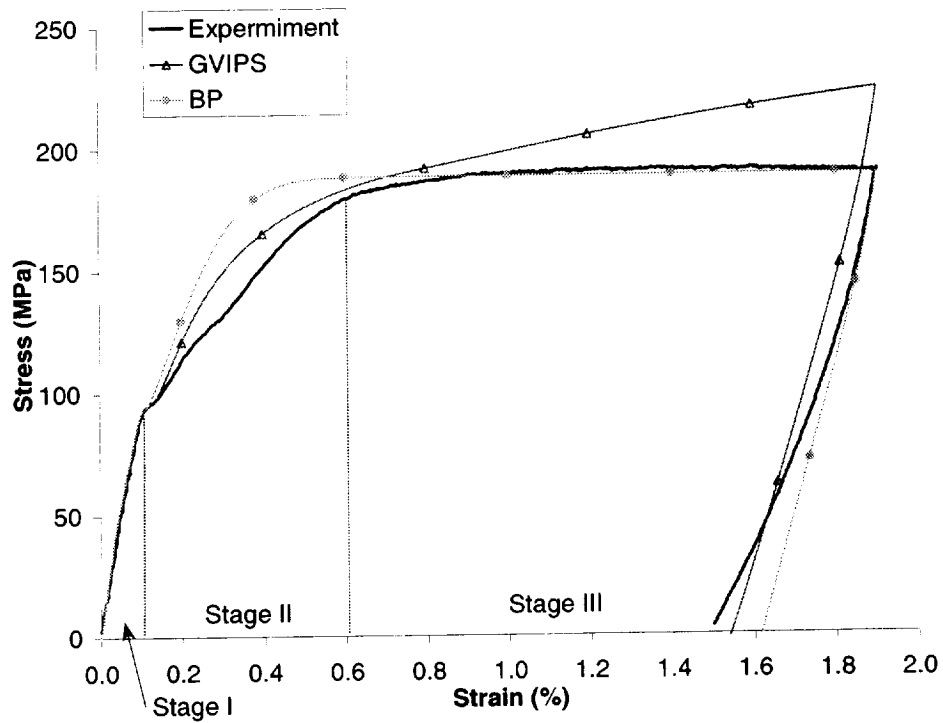


Figure 23: Predicted and experimental response of 20% SCS-6 TIMETAL 21S at 650 °C. The effect of matrix constitutive model is highlighted. The ECI debonding model was employed. $\dot{\epsilon} = 10^{-4} \text{ s}^{-1}$.

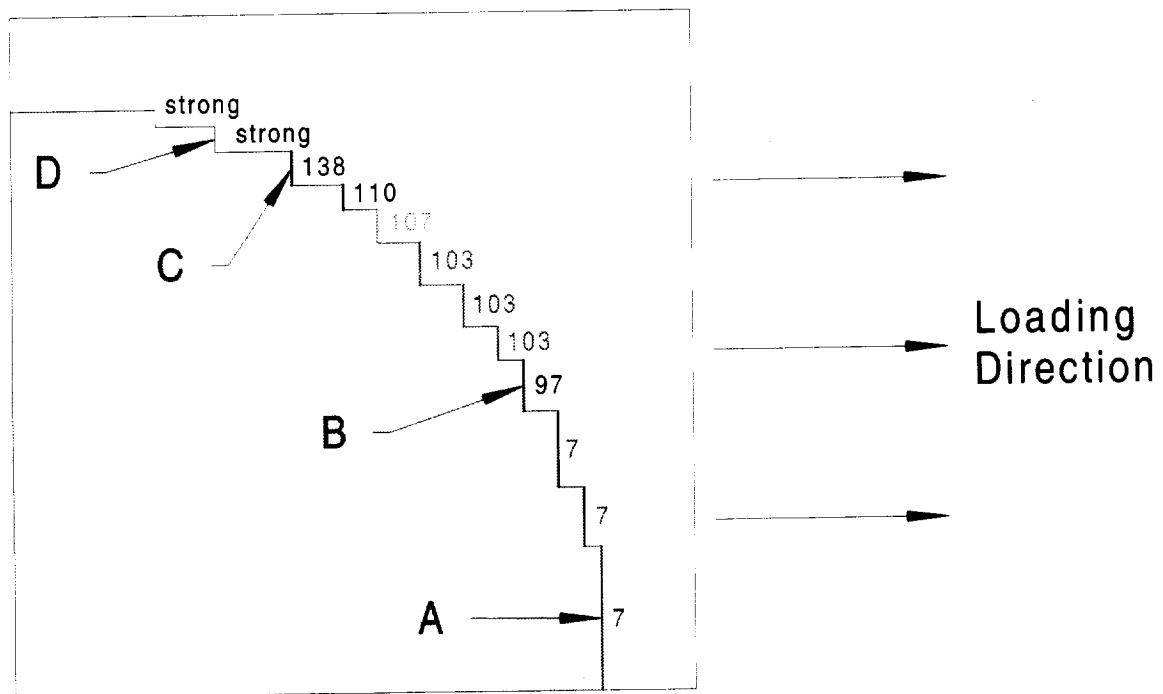


Figure 24: Interfacial debond strengths used for simulations with the BP matrix constitutive model.

As Fig. 23 indicates, the predictions made using **GVIPS** are in better agreement with experimental results in Stage II (where the effects of interfacial debonding dominate the composite response), whereas the predictions made using **BP** are in better agreement with experiment in Stage III. These results are completely consistent with the characteristics of the two constitutive models used to represent the matrix only response (see Fig. 13). Consequently, in order to obtain excellent agreement with experiment in all stages, it is necessary to have not only a realistic debonding model, but also a highly accurate matrix constitutive model that is well representative for all stages of deformation. It seems that in order to further improve the accuracy of the **MAC/GMC** simulations for the transverse tensile response of SCS-6/TIMETAL 21S, improved characterization of the **GVIPS** model for TIMETAL 21S is necessary. To this end, work is ongoing to develop a new multimechanism **GVIPS** formulation which is significantly more accurate (e.g. see Saleeb et al., 2000).

Pure predictions for the transverse tensile behavior of TMCs using **MAC/GMC** in conjunction with the new debonding model are problematic. As discussed in Section 3, the simulated interfacial behavior is greatly affected by the percentage of the unit cell cross-section that debonds, the strain rate, and the matrix constitutive behavior. One of the ways that the matrix constitutive model dependence is manifested is in the significant temperature-dependence of the modeled interfacial response. In order to render the **ECI** model sufficiently robust to make accurate pure predictions for the transverse tensile response of an MMC system, the model parameters would require characterization based on all of the aforementioned influencing factors. As discussed in Section 6.3, compensation for the strain rate effect is easy. The remaining influencing factors, on the other hand, are not so easily handled. This point becomes clear when attempts are made to apply the model to the same material system (SCS-6/TIMETAL 21S) with different fiber volume fractions, unit cell aspect ratios, or temperatures while using the same debond model parameters. Figure 25 compares the predicted tensile response of 30% SCS-6/TIMETAL 21S having a unit cell aspect ratio (in the laminate core, see Fig. 16) of 1.0 with experimental data. The **GVIPS** matrix constitutive model was employed, as were the debonding model

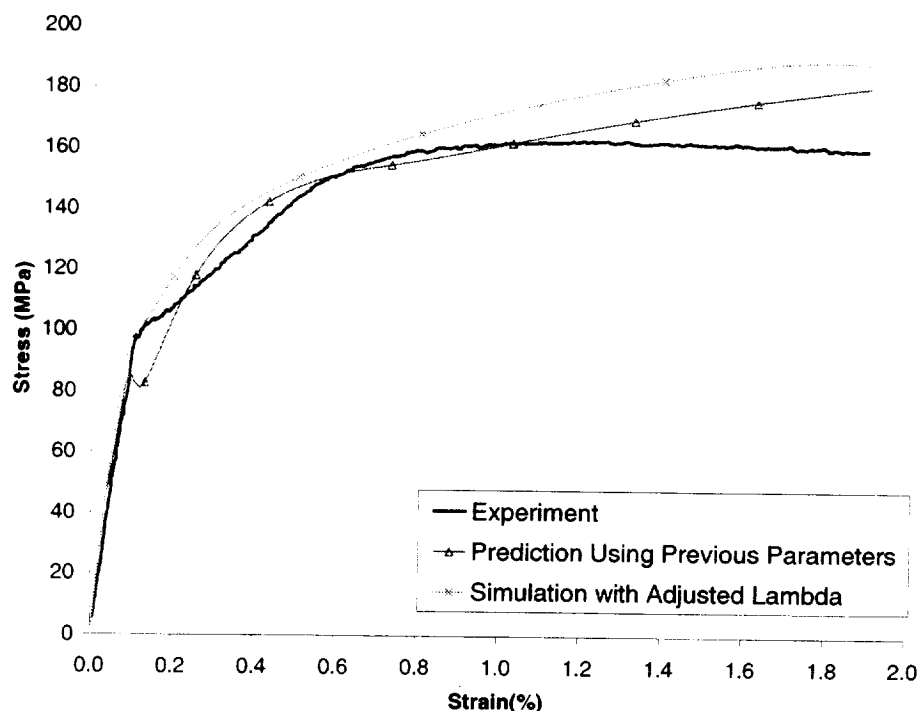


Figure 25: Simulated and experimental transverse tensile response of 30% SCS-6/TIMETAL 21S at 650 °C with $R = 1.0$ and $\dot{\epsilon} = 10^{-4} \text{ sec}^{-1}$. The **GVIPS** matrix constitutive model was employed.

parameters characterized based on the 20% SCS-6/TIMETAL 21S having a core aspect ratio of 0.82. Tests on both composites were performed at a strain rate of 10^{-4} sec^{-1} and a temperature of 650 °C. The overall agreement between the prediction and experiment is fair. However, since the higher fiber volume fraction and core aspect ratio of the composite modeled in Fig. 25 lead to debonding of a larger overall percentage of the unit cell cross-section (as well as a larger cross-section per failure event), an unrealistic “dip” is present in the predicted stress-strain curve. By adjusting the value of Λ at each interface to $\frac{1}{4}$ of its previous value, the second much more realistic simulation shown in Fig. 25 was made.

Predictions for SCS-6/TIMETAL 21S at temperatures other than 650 °C are not presented. Attempts to fully characterize the ECI model parameters based on debonding event cross-section (determined by fiber volume fraction and repeating unit cell aspect ratio) and temperature, while unsuccessful, led to the examination of the matrix constitutive model. We believe that the current difficulty associated with using the model for pure predictions is attributable mainly to inaccuracies in the matrix constitutive model characterization, which causes inaccuracies in the residual stress field. Altering the composite configuration or temperature also causes significant (nonlinear) changes in the simulated residual stress field. Thus, it appears that accurate pure predictions for the transverse tensile response of SiC/Ti will hinge on the availability of higher fidelity nonisothermal viscoplastic constitutive models and model parameters. It should be noted that, at some point, the accuracy of the predictions may be limited by GMC's lack of shear coupling and geometrical limitations. However, as shown by Bednarczyk and Arnold (2000), these limitations can often be overcome with a little ingenuity. Finally, it should be noted that, although pure predictions are not presently possible, the ECI model parameters can be selected to provide good correlation with experiment at any temperature, fiber volume fraction, or fiber packing arrangement. Thus, were sufficient data available, it would be possible to correlate the parameters for a number of composite configurations and temperatures and interpolate to arrive at parameters for use in predictions for any general case.

7.2 Transverse Creep

Model simulations were also performed for the transverse creep behavior of the 20% SCS-6/TIMETAL 21S composite (at 650 °C) according to which the ECI model parameters were characterized. These simulations provide insight into the ECI model's ability to transcend the type of loading for which its parameters were originally selected. Eggleston (1993) examined the transverse creep of SiC/Ti-6-4 using finite element analysis (FEA) in conjunction with interfacial debonding modeling. This study showed that the composite creep behavior could be bounded by FEA with simulated perfect bonding and FEA with simulated complete debonding. Further, Eggleston (1993) included the NI model in the FEA analysis, but the resulting transverse creep simulations were in poor agreement with experiment. These simulations suffered not only from difficulties associated with the NI model (see Section 3.3) but also from inaccuracies in the employed matrix constitutive model.

Figure 26 shows experimental transverse creep data for a 20% SCS-6/TIMETAL 21S composite at 650 °C with an applied load of 55 MPa. The specimen on which this test was performed was cut from the same plate as the tensile test specimen whose response was used for characterization of the ECI model parameters (see Figs. 15, 21, and 22). Four stages of the composite's creep response have been identified in Fig. 26, along with theoretical mechanisms, which are proposed to explain the observed behavior. It should be noted that *these stages are not characteristic of the composite's transverse creep response in general*. As illustrated by Eggleston (1993) and Bowman (1999), variations in fiber volume fraction, applied stress level, and temperature can significantly affect the qualitative appearance of SiC/Ti composites' transverse creep response.

In Fig. 26, the stage I creep response is nonlinear and resembles the primary creep regime apparent in the 650 °C TIMETAL 21S matrix creep response (Fig. 14). Thus the stage I response of the composite has been attributed to primary creep in the matrix along with a proposed partial interfacial debonding mechanism. The stage II behavior is linear in nature and resembles the steady-state creep regime observed in the TIMETAL 21S creep response (Fig. 14). Since the composite creep response is

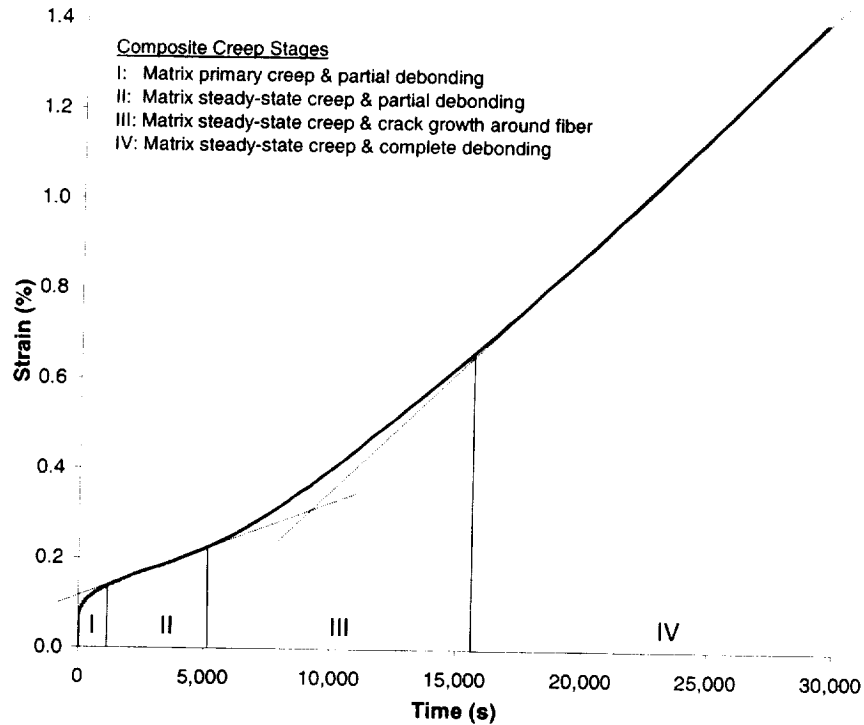


Figure 26: Experimental transverse creep response of 20% SCS-6/TIMETAL 21S at 650 °C to an applied stress of 55 MPa.

linear, this stage has been attributed to steady-state matrix creep coupled with the same degree of partial interfacial debonding as in stage I. That is, in stage II, the interfacial debonding does not progress noticeably. In stage III, the composite transverse creep response is nonlinear as the creep rate increases significantly, possibly indicating the onset of tertiary creep in the matrix. However, the linear stage IV (along with the fact that the composite does not soon fail after stage III) suggests another mechanistic explanation. We suggest that this nonlinear stage III transition between two linear stages is brought about by slow growth of interfacial cracks around the fibers. That is, in stage III, the debonding progresses from its initial (stage I) extent to a completely debonded state, while the matrix creep continues its typical steady-state character. Then, the linear stage IV corresponds to continued matrix steady-state creep coupled with completely debonded interfaces, a state similar to a creeping slab of TIMETAL 21S with holes. Note that the creep experiment depicted in Fig. 26 was not taken to failure; the specimen continued its stage IV character until the test was interrupted at approximately 60,000 seconds.

Figure 27 provides a comparison of model simulations with the experimental transverse creep response shown in Fig. 26. Predictions were made using **GVIPS** with the **CCI** model, **BP** with the **ECI** model, and **GVIPS** with the **ECI** model, where the previously characterized model parameters were employed. An additional simulation was performed using **GVIPS** with the **ECI** model in which the **ECI** model parameters were adjusted. The applied stress level in the experiment and simulations in Fig. 27 was 55 MPa, which, in the case of the model predictions, leads to debonding of only the weakest interfaces. The fact that the model predicts partial interfacial debonding during the application of the mechanical loading lends credence to mechanistic explanations for stages I and II. For the predictions using **GVIPS** with the **CCI** and **ECI** models, only the two interfaces with strengths of 41 MPa debond (see Fig. 17), while for the prediction using **BP**, only the three interfaces with strengths of 7 MPa debond (see Fig. 24). The final simulated creep curve was generated by altering the **ECI** model parameters, allowing the weakest five interfaces (see Fig. 17) to debond during application of the 55 MPa tensile load, and allowing all remaining interfaces to debond later in the simulated creep test.

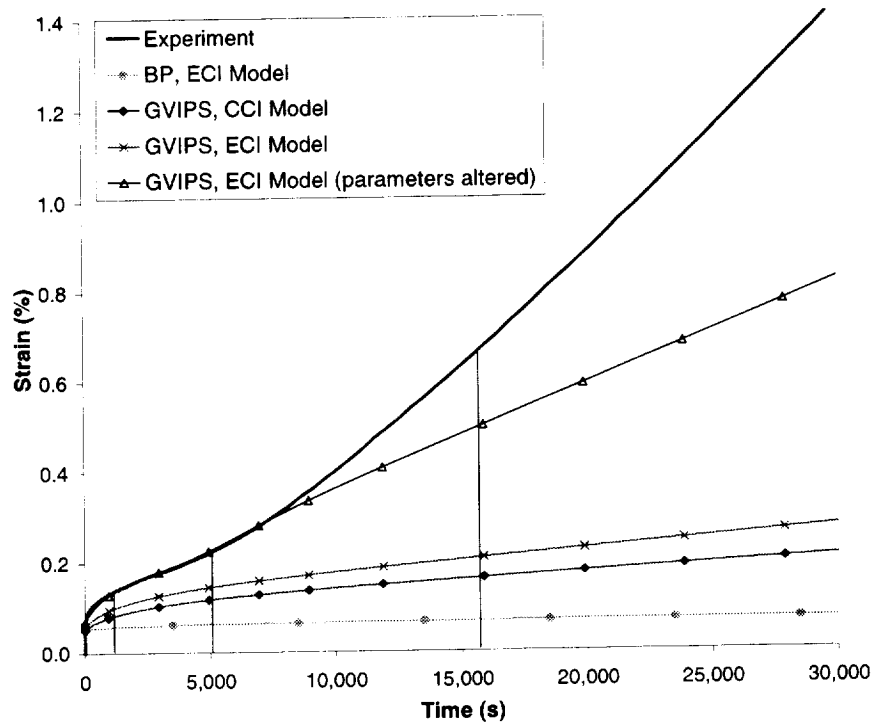


Figure 27: Predicted, simulated, and experimental transverse creep response of 20% SCS-6/TIMETAL 21S at 650 °C to an applied stress of 55 MPa.

Fig. 27 indicates that, while all of the simulations in which the parameters were not altered underpredict the experimental creep response of the composite, the simulation performed using **GVIPS** with the **ECI** model was the most accurate of these. Recall from Fig. 14 that some of the discrepancy between this prediction and experiment can be attributed to insufficient characterization of the matrix creep behavior at lower stress levels. The greater amount of creep that is predicted using the **ECI** model compared to the **CCI** model (both with **GVIPS**) is caused by the redistribution of unloaded stress to intact matrix regions that occurs with the **ECI** model. These intact matrix regions then experience higher local stress levels (compared to simulations performed using the **CCI** model) and consequently creep to a greater extent. The **GVIPS** matrix constitutive model is significantly more realistic than **BP** for the transverse creep of SiC/Ti composites. Even when employed in conjunction with the **ECI** model, the **BP** model predicts steady-state creep immediately and significantly underpredicts the experimental creep curve.

Clearly, the simulation that was performed after recalibrating the **ECI** model provides the best agreement with the experimental transverse creep response (Fig. 27). For this case, five interfaces were given low bond strengths (41 MPa) so they debonded during the application of the 55 MPa tensile load and then quickly unloaded. This allows the simulation to agree well with experiment in stages I and II. To achieve better agreement in stage III, all remaining simulated interfaces were permitted to debond in turn and slowly unload their stress (via alteration of the **ECI** model parameter B) to simulated crack growth around the fiber. For these interfaces, an altered value of $B = 4598 \text{ s}$ was determined by using eqn (6) in conjunction with $B_{\text{ref}} = 10 \text{ s}$, $\dot{\epsilon}_{\text{ref}} = 10^{-4} \text{ s}^{-1}$, and the measured stage II global strain rate, $\dot{\epsilon} = 2.175 \times 10^{-7} \text{ s}^{-1}$. Thus, the simulated process is one in which the fiber-matrix interface debonds to an angle of approximately 37° during application of the 55 MPa mechanical load. Then the interface unzips

slowly (and completely) during stage III, simulating the suggested slow crack growth at the fiber matrix interface around the fiber. At times greater than approximately 8000 s, the simulation still underpredicts the experimental creep response. This discrepancy is likely due to inaccuracies in the matrix constitutive model (see Fig. 14) coupled with the inability of the model to simulate accurately the stress concentrations associated with the stage IV holes in the matrix.

Figure 28 shows the predicted creep behavior of the same 20% SCS-6/TIMETAL 21S composite with an applied stress of 124 MPa. Note that experimental data for this case were unavailable and that no recalibration of the **ECI** model parameters was performed. At this higher applied stress level all simulated interfaces that are permitted to debond do so during the applied mechanical loading for both matrix constitutive models (see Figs. 17 and 24). Note that, under this condition, one would not expect to see the stage III regime that was observed in Figs. 26 and 27, since the interfaces have already debonded to their full extent. In Fig. 28, the amount of creep predicted when employing the **BP** model with the **ECI** model is significantly greater than that predicted using **GVIPS** with the **ECI** debonding model. This is consistent with the creep simulations for the pure TIMETAL 21S matrix performed using the two constitutive models at the high-applied stress level (see Fig. 14). The creep curve predicted using **GVIPS** with the **ECI** model is significantly higher than that predicted using **GVIPS** with the **CCI** model. Once again, the redistribution of stress associate with unloading in the **ECI** model has lead to an increase in the composite creep response. Of the curves plotted, it is likely that the creep simulation performed using **GVIPS** and the **ECI** model would compare most favorably with experimental data were it available for inclusion in Fig. 28. Like the transverse tensile simulations, the transverse creep simulations for the composite would improve if the matrix viscoplastic constitutive model were improved.

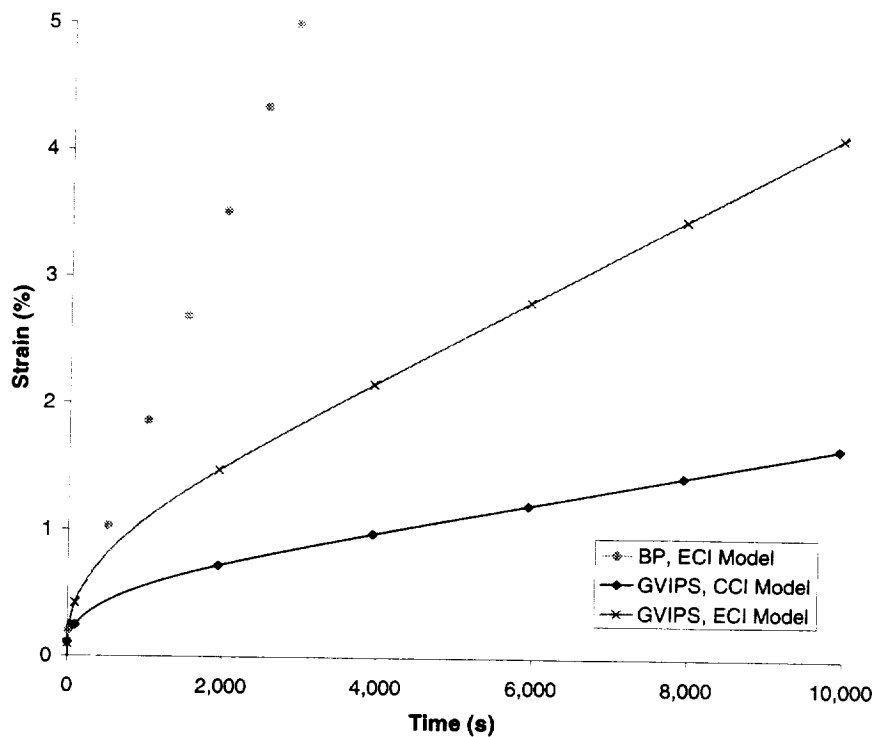


Figure 28: Predicted transverse creep response of 20% SCS-6/TIMETAL 21S at 650 °C to an applied stress of 124 MPa.

8. Summary/Conclusion

A new local debonding model has been developed, implemented, and applied to simulate the transverse tensile and creep behavior of SCS-6/TIMETAL 21S composites. It is based on an existing flexible interface model, but unlike its direct predecessors, the new **ECI** model allows debonding to progress via unloading of the interfacial stress after debonding occurs. This unloading was enabled by incorporation of explicit time-dependence into parameters controlling the effective interfacial compliance. Further, unlike previous approaches to modeling debonding that do permit interfacial stress unloading, the **ECI** model requires solution of no additional equations (in the micromechanics model), includes a finite interfacial bond strength, and does not require accuracy-reducing simplifying assumptions to facilitate its implementation. The **ECI** model thus provides a unique combination of physical accuracy, simplicity, and efficiency. The **ECI** model has been incorporated into NASA's **MAC/GMC** software package, thus allowing it to be employed in a wide range of simulations.

Simulations of the transverse tensile response of SCS-6/TIMETAL 21S composites were made using a realistic geometric representation of the actual composite configuration. By choosing the empirical debonding parameters wisely, accurate simulation of the composite tensile response was obtained. In order to enable pure prediction of the composite response for a wide range of composite configurations and temperatures (without recalibrating the empirical parameters), characterization of the debonding parameters to account for these effects would be necessary. Attempts to perform this characterization demonstrated the need for a higher level of accuracy from the matrix viscoplastic constitutive representations than is available at this time. Constitutive model inaccuracies were also shown to have a dominant impact on the model's ability to accurately predict the transverse creep of SCS-6/TIMETAL 21S. As with tension, the creep predictions were significantly improved via use of the new **ECI** model, and still better agreement was achieved via alteration of the **ECI** model parameters to account more realistically for the postulated mechanisms (e.g. creep crack growth) in the four stages of the measured creep response.

This study has clearly demonstrated the need for improvements in the viscoplastic constitutive models available for TIMETAL 21S in order to predict the transverse response of SCS-6/TIMETAL 21S. Accordingly, the **GVIPS** constitutive model parameters employed for the matrix are in the process of being reworked so that the model can more accurately span a larger stress, time, and temperature domain. Upon completion of this effort, effects associated with the debonding model will be isolated from those associated with matrix constitutive model, and the new **ECI** debonding model presented herein will be revisited to characterize the model. The model will then be sufficiently robust to enable the accurate prediction of the interfacial debonding effects in a wide range of weakly bonded composites. This accurate simulation technology is necessary to aid development of the accurate design and life prediction tools that are needed to facilitate the implementation of advanced composite materials.

References

- Aboudi, J. (1987) "Damage in Composites – Modeling of Imperfect Bonding" *Composites Science and Technology*. Vol. 28, pp. 103-128.
- Aboudi, J. (1991) *Micromechanics of Composite Materials: A Unified Micromechanical Approach*. Elsevier, Amsterdam.
- Aboudi, J. (1995) "Micromechanical Analysis of Thermo-Inelastic Multiphase Short-Fiber Composites" *Composites Engineering*. Vol. 5, No. 7, pp. 839-850.
- Achenbach, J.D. and Zhu, H. (1989) "Effect of Interfacial Zone on Mechanical Behavior and Failure of Fiber-Reinforced Composites" *Journal of the Mechanics and Physics of Solids*. Vol. 37, No. 3, pp. 381-393.
- Arnold, S.M., Bednarczyk, B.A., Wilt, T.E., and Trowbridge, D. (1999) "MAC/GMC User Guide: Version 3.0" *NASA/TM-1999-209070*.
- Arnold, S.M., Pindera, M.-J., and Wilt, T.E. (1996a) "Influence of Fiber Architecture on the Inelastic Response of Metal Matrix Composites" *International Journal of Plasticity*. Vol. 12, No. 4, pp. 507-545.
- Arnold, S.M. and Saleeb, A.F. (1994) "On the Thermodynamic Framework of Generalized Coupled Thermoelastic-Viscoplastic-Damage Modeling" *International Journal of Plasticity*. Vol. 10, No. 3, pp. 263-278.
- Arnold, S.M., Saleeb, A.F., and Castelli, M.G. (1996b) "A Fully Associative, Nonisothermal, Nonlinear Kinematic, Unified Viscoplastic Model for Titanium Alloys" in *Thermo-Mechanical Fatigue Behavior of Materials: Second Volume*. M.J. Verrilli and M.G. Castelli (eds.), ASTM STP-1263, American Society for Testing and Materials, Philadelphia, pp. 146-173.
- Arnold, S.M., Saleeb, A.F., and Castelli, M.G. (1996c) "A Fully Associative, Nonlinear Kinematic, Unified Viscoplastic Model for Titanium Based Matrices" in *Life Prediction Methodology for Titanium Matrix Composites*. W.S. Johnson, J.M. Larsen, and B.N. Cox (eds.), ASTM STP-1253, American Society for Testing and Materials, Philadelphia, pp. 231-256.
- Bednarczyk, B.A. and Arnold, S.M. (2000) "A New Local Failure Model With Application to the Longitudinal Tensile Behavior of Continuously Reinforced Titanium Composites" *NASA/TM-2000-210027*.
- Bednarczyk, B.A. and Pindera, M.-J. (2000) "Inelastic Response of a Woven Carbon/Copper Composite – Part II: Micromechanics Model" *Journal of Composite Materials*. Vol. 34, No. 4, pp. 299-331.
- Bowman, C.L. (1999) "Experimentation and Analysis of Mechanical Behavior Modification of Titanium Matrix Composites Through Controlled Fiber Placement" Ph.D. Dissertation, Case Western Reserve University.
- Brindley, P.K. and Draper, S.L. (1993) "Failure Mechanisms of 0° and 90° SiC/Ti-24Al-11Nb Composites Under Various Loading Conditions" *Structural Intermetallics*. R. Darolia et al. (eds.), The Minerals, Metals & Materials Society, pp. 727-737.

- Cervay, R.R. (1994) "SCS-6/ β 21s and SCS-9/ β 21s Mechanical Property Evaluation" *NASP Contractor Report 1165*. Wright-Patterson Air Force Base, Ohio.
- Chan, K.S., Bodner, S.R., and Lindholm, U.S., (1988) "Phenomenological Modeling of Hardening and Thermal Recovery in Metals" *Journal of Engineering Materials and Technology*. Vol. 110, pp. 1-8.
- Chan, K.S. and Lindholm, U.S., (1990) "Inelastic Deformation Under Nonisothermal Loading" *Journal of Engineering Materials and Technology*. Vol. 112, pp. 15-25.
- Eggleston, M.R. (1993) "Testing, Modeling and Analysis of Transverse Creep in SCS-6/Ti-6Al-4V Metal Matrix Composites at 482 °C" *GE Research & Development Center Report 93CRD163*.
- Goldberg, R.K. and Arnold, S.M. (2000) "A Study of Influencing Factors on the Tensile Response of a Titanium Matrix Composite With Weak Interfacial Bonding" *NASA/TM-2000-209798*.
- Hu, S. (1996) "The Transverse Failure of a Single-Fiber Metal-Matrix Composite: Experiment and Modeling" *Composites Science and Technology*. Vol. 56, pp. 667-676.
- Jones, J.P., and Whittier, J.S. (1967) "Waves at Flexibly Bonded Interfaces" *Journal of Applied Mechanics*. Vol. 34, pp. 905-909.
- Karlak, R.F., Crossman, F.W., and Grant, J.J. (1974) "Interface Failures in Composites" *Proc. Failure Modes in Composites II*. Pittsburgh, Pa., Metallurgical Society of AIME, New York.
- Kroupa J.L. (1993) "Implementation of a Nonisothermal Unified Inelastic-Strain Theory Into ADINA6.0 for a Titanium Alloy - User Guide" *Wright Laboratory Report WL-TR-93-4005*. University of Dayton, Dayton, Ohio.
- Lerch, B.A. and Saltsman, J.F. (1993) "Tensile Deformation of SiC/Ti-15-3 Laminates" in *Composite Materials: Fatigue and Fracture: Fourth Volume*. W.W. Stinchcomb and N.E. Ashbaugh (eds.), ASTM STP 1156, American Society for Testing and Materials, Philadelphia, pp. 161-175. See also *NASA TM 103620*.
- Majumdar, B.S. and Newaz, G.M. (1992) "Inelastic Deformation of Metal Matrix Composites: Plasticity and Damage Mechanisms" *Philosophical Magazine A*. Vol. 66, No. 2, pp. 187-212. See also *NASA CR-189095*.
- McGee, J.D. and Herakovich, C.T. (1992) "Micromechanics of Fiber/Matrix Debonding" *Report AM-92-01*. Applied Mechanics Program, University of Virginia, Charlottesville, Va.
- Needleman, A. (1987) "A Continuum Model for Void Nucleation by Inclusion Debonding" *Journal of Applied Mechanics*. Vol. 54, pp. 525-531.
- Neu, R.W. (1993) "Nonisothermal Material Parameters For the Bodner-Partom Model" *Material Parameter Estimation for Modern Constitutive Equations*. MD - Vol. 43, L.A. Betram, S.B. Brown, and A.D. Freed (eds.), ASME Book No. H00848.
- Nimmer, R.P., Bankert, R.J., Russell, E.S., Smith, G.A., and Wright, K. (1991) "Micromechanical Modeling of Fiber/Matrix Interface Effects in Transversely Loaded SiC/Ti-6-4 Metal Matrix Composites" *Journal of Composites Technology and Research*. Vol. 13, No. 1, pp. 3-13.

- Pindera, M.-J. and Bednarczyk, B.A. (1999) "An Efficient Implementation of the Generalized Method of Cells for Unidirectional, Multi-Phased Composites with Complex Microstructures" *Composites Part B*. Vol. 30, No. 1, pp. 87-105.
- Robertson, D.D. and Mall, S. (1994) "Micromechanical Analysis of Metal Matrix Composite Laminates With Fiber/Matrix Interfacial Damage" *Composites Engineering*. Vol. 4, No. 12, pp. 1257-1274.
- Saleeb, A.F., Arnold, S.M., Castelli, M.G., Wilt, T.E., and Graf, W. (2000) "A General Hereditary Multimechanism-Based Deformation Model with Application to the Viscoelastoplastic Response of Titanium Alloys" *International Journal of Plasticity*. In press.
- Warrier, S.G., Rangaswamy, P., Bourke, M.A.M., and Krishnamurthy, S. (1999) "Assessment of the Fiber/Matrix Interface Bond Strength in SiC/Ti-6Al-4V Composites" *Materials Science and Engineering*. Vol. A259, pp. 220-227.
- Wilt, T.E. and Arnold, S.M. (1996) "Micromechanics Analysis Code (MAC) User Guide: Version 2.0" *NASA TM-107290*.
- Wilt, T.E., Arnold, S.M., and Saleeb, A.F. (1997) "A Coupled/Uncoupled Computational Scheme for Deformation and Fatigue Damage Analysis of Unidirectional Metal-Matrix Composites" in *Applications of Continuum Damage Mechanics to Fatigue and Fracture*. D.L. McDowell (ed.), ASTM STP 1315, American Society for Testing and Materials, Philadelphia, pp. 65-82.

REPORT DOCUMENTATION PAGE			Form Approved OMB No. 0704-0188	
Public reporting burden for this collection of information is estimated to average 1 hour per response, including the time for reviewing instructions, searching existing data sources, gathering and maintaining the data needed, and completing and reviewing the collection of information. Send comments regarding this burden estimate or any other aspect of this collection of information, including suggestions for reducing this burden, to Washington Headquarters Services, Directorate for Information Operations and Reports, 1215 Jefferson Davis Highway, Suite 1204, Arlington, VA 22202-4302, and to the Office of Management and Budget, Paperwork Reduction Project (0704-0188), Washington, DC 20503.				
1. AGENCY USE ONLY (Leave blank)	2. REPORT DATE August 2000	3. REPORT TYPE AND DATES COVERED Technical Memorandum		
4. TITLE AND SUBTITLE A New Local Debonding Model With Application to the Transverse Tensile and Creep Behavior of Continuously Reinforced Titanium Composites		5. FUNDING NUMBERS WU-242-23-52-00		
6. AUTHOR(S) Brett A. Bednarczyk and Steven M. Arnold				
7. PERFORMING ORGANIZATION NAME(S) AND ADDRESS(ES) National Aeronautics and Space Administration John H. Glenn Research Center at Lewis Field Cleveland, Ohio 44135-3191		8. PERFORMING ORGANIZATION REPORT NUMBER E-12226		
9. SPONSORING/MONITORING AGENCY NAME(S) AND ADDRESS(ES) National Aeronautics and Space Administration Washington, DC 20546-0001		10. SPONSORING/MONITORING AGENCY REPORT NUMBER NASA TM-2000-210029		
11. SUPPLEMENTARY NOTES Brett A. Bednarczyk, Ohio Aerospace Institute, 22800 Cedar Point Road, Brook Park, Ohio 44142; and Steven M. Arnold, NASA Glenn Research Center. Responsible person, Steven M. Arnold, organization code 5920, (216) 433-3334.				
12a. DISTRIBUTION/AVAILABILITY STATEMENT Unclassified - Unlimited Subject Categories: 24 and 39 This publication is available from the NASA Center for AeroSpace Information, (301) 621-0390.		12b. DISTRIBUTION CODE Distribution: Nonstandard		
13. ABSTRACT (Maximum 200 words) A new, widely applicable model for local interfacial debonding in composite materials is presented. Unlike its direct predecessors, the new model allows debonding to progress via unloading of interfacial stresses even as global loading of the composite continues. Previous debonding models employed for analysis of titanium matrix composites are surpassed by the accuracy, simplicity, and efficiency demonstrated by the new model. The new model was designed to operate seamlessly within NASA Glenn's Micromechanics Analysis Code with Generalized Method of Cells (MAC/GMC), which was employed to simulate the time- and rate-dependent (viscoplastic) transverse tensile and creep behavior of SiC/Ti composites. MAC/GMC's ability to simulate the transverse behavior of titanium matrix composites has been significantly improved by the new debonding model. Further, results indicate the need for a more accurate constitutive representation of the titanium matrix behavior in order to enable predictions of the composite transverse response, without resorting to recalibration of the debonding model parameters.				
14. SUBJECT TERMS Elastic; Viscoplasticity; Deformation; Metal matrix composites, Interfacial debonding		15. NUMBER OF PAGES 40		
		16. PRICE CODE A03		
17. SECURITY CLASSIFICATION OF REPORT Unclassified	18. SECURITY CLASSIFICATION OF THIS PAGE Unclassified	19. SECURITY CLASSIFICATION OF ABSTRACT Unclassified	20. LIMITATION OF ABSTRACT	

